Page 7 of 47 Nanoscale

## Effect of solvent quality and sidechain architecture on the conjugated polymer chain conformation in solution

Guorong Ma<sup>1</sup>, Zhaofan Li<sup>2</sup>, Lei Fang<sup>3</sup>, Wenjie Xia<sup>2</sup>, Xiaodan Gu<sup>1\*</sup>

- 1. School of Polymer Science and Engineering, The University of Southern Mississippi, Hattiesburg, MS, 39406, USA
- 2. Department of Aerospace Engineering, Iowa State University, Ames, IA 50011, USA
- 3. Department of Chemistry, Texas A&M University, College Station, TX 77843, USA Correspondence to: Xiaodan Gu (Email: xiaodan.gu@usm.edu)

*Keywords*: conjugated polymers, poly (thiophene), static light scattering, second virial coefficient, solvent quality, chain conformation

#### 1 Abstract

Conjugated polymers (CPs) are solution-processible for various electronic applications, where solution aggregation and dynamics could impact the morphology in the solid state. Various solvents and solvent mixtures have been used to dissolve and process CPs, but few studies quantify the effect of solvent quality on the solution behaviors of CPs. Here, we performed static light scattering, small-angle X-ray scattering, combined with molecular dynamics (MD) simulation, to investigate CPs solution behaviors with various solvent quality, including poly(3-alkylthiophene) (P3ATs) with various sidechain lengths from -C<sub>4</sub>H<sub>9</sub> to -C<sub>12</sub>H<sub>25</sub>, poly[bis(3-dodecyl-2-thienyl)-2,2'dithiophene-5,5'-diyl] poly[2,5-bis(3-dodecylthiophen-2-yl)thieno[3,2-(PQT-12) and b]thiophene] (PBTTT-12). We found that chlorobenzene is a better solvent than toluene for various CPs. It is evident from the majority positive second virial coefficient  $A_2$  ranging from 0.3 to 4.7 ×10<sup>-3</sup> cm<sup>3</sup>\*mol/g<sup>2</sup> towards P3ATs. For P3ATs in non-polar solvents, longer sidechains promote more positive  $A_2$  and thus signaling a better polymer-solvent interaction, where in toluene  $A_2$ increases from -5.9 to  $1.4 \times 10^{-3}$  cm<sup>3</sup>\*mol/g<sup>2</sup> and in CB  $A_2$  ranges from 1.0 to  $4.7 \times 10^{-3}$  cm<sup>3</sup>\*mol/g<sup>2</sup>

Nanoscale Page 8 of 47

when sidechain length increases from  $-C_6H_{13}$  to  $-C_{12}H_{25}$ . Moreover, PQT-12 and PBTTT-12 have strong aggregation tendencies in all the solutions, with an apparent positive  $A_2$  ( $\sim 0.5 \times 10^{-3}$  cm<sup>3</sup>\*mol/g<sup>2</sup>) due to multi-chain aggregates and peculiar chain folding. These solvent-dependent aggregation behaviors can be well correlated to spectroscopy measurement results. Our coarse-grained MD simulation results further suggested that CPs with longer, dense, and branched sidechain can achieve enhance polymer-solvent interaction, and thus enable overall better solution dispersion. Our work here provides quantitative insights into the solution behavior of conjugated polymers that can guide both the design and process of CPs toward next-generation organic electronics.

#### 2 Introduction

Numerous innovative electronic devices have demonstrated novel applications with remarkable efficiency, sensitivity, and mobility, such as organic photovoltaics (OPV), organic electrochemical transistors (OECT), and organic field effect transistors (OFET). The active layer of these devices commonly comprises organic materials, including small molecules or conjugated polymers (CPs). CPs offer a host of advantages, such as intrinsic stretchability, environmental stability, adjustable energy levels, and solution processability, owing to their versatile chemical structure through coupling synthesis. Generally, CPs feature a continuous delocalized electrons distribution along the backbone for efficient charge transport, alongside short dispersed sidechains to enhance solubility. In practice, longer sidechains and higher temperatures have been observed to improve solubility for many CPs, in addition to the choice of suitable solvents. Nonetheless, a systematic comparison in this regard is currently lacking to elucidate the solvent quality effect.

To preserve conductive pathways along the backbone, chain conformation is crucial where a rigid and coplanar backbone is ideal.<sup>7, 8</sup> The way CPs are arranged in the solid state significantly affects their electronic and optoelectronic properties, making the solution behavior a critical aspect of processing CP-based devices. The behavior of the polymer chains in the solution phase directly impacts their packing in the solid state. This includes factors such as solubility, chain conformation, and interactions between polymer chains. CPs can be dispersed in solution into small aggregates, fully dissolved single chains, or a mixture of both.<sup>9</sup> These heterogeneous state of CPs in the solution depends on solvent quality and temperatures, yielding drastically different particle sizes and dynamics.<sup>9</sup> Upon aging, doping, or adding antisolvent, CPs can form multichain aggregates from dissolved solution, where aggregates' shape can vary from long fibers to spherical

Page 9 of 47 Nanoscale

aggregates. <sup>10, 11, 12</sup> CPs chain conformation can be probed by small-angle scattering, using X-ray, neutron, or laser light. <sup>12-14</sup> Overall, CPs chain conformation and aggregation behavior in solution can be effectively controlled by solvent selection besides optimal processing conditions.

Numerous studies have concentrated on manipulating chain conformation and pre-aggregate formation by employing a range of solvents or solvent mixtures. 15 These solvents possess diverse characteristics including solubility, toxicity, boiling point, viscosity, and polarity. 16, 17 Gregory et al. investigated the gelation of poly(3-alkylthiophene)s (P3ATs) in a mixture of good and poor solvents. 18 They found that for P3HT in dichlorobenzene, more poor-solvent n-dodecane results in smaller, abundant fiber formation and better electrical conductivity. Chang et al. investigated the solvent-addictive acetone effect on the precursor solution of P3HT in chloroform. <sup>19</sup> The 4-fold increase in charge mobility is attributed to the acetone-chloroform complex which has a lower evaporation rate. Lee et al. investigated a donor-acceptor fused thiophene-diketopyrrolopyrrole copolymer (PTDPPTFT4) the chain conformation of in solvent mixture of tetrahydronaphthalene and p-xylene. <sup>20</sup> The increase of p-xylene leads to a higher degree of aggregation along with a more oriented film due to non-polar p-xylene's weak interaction with the polar backbone. The rigid aggregation fraction was confirmed by SAXS. Kwok et al. studied the chain conformation of isoindigo-bithiophene-based polymer (PII-2T) in a chlorobenzene and decane mixture.<sup>21</sup> All polymer solutions contain fibril and dispersed single chains at various concentrations (1-20 mg/ml), leading to complex modeling which requires careful data analysis for solution scattering. Xi et al. investigated the morphology of poly[2,5-(2-octyldodecyl)-3,6-diketopyrrolopyrrole-alt-5,5-(2,5-di(thien-2-yl))thieno[3,2b]thiophene] (DPPDTT) aggregates using small-angle neutron scattering. 11 By adding 5-20 v% poor solvent methanol and dimethyl sulfoxide (DMSO) into good solvent chloroform, they found chain rigidity change upon adding poor solvents, depending on the polarity of poor solvents. However, in terms of the interaction between polymer and solvent, these works did not focus their discussion on solvent quality.

Traditionally, solvent quality can be estimated by Hansen solubility parameters (HSP), where the cohesive energy between solute and solvent can be separated into dispersion, polarity, and hydrogen bonds.<sup>22</sup> It has been used to optimize solvent for CPs<sup>17, 23</sup> and predict the phase separation of donor and acceptor blend of OPV devices.<sup>7, 24</sup> Machui *et al.* measured the HSP values of P3HT and PCBM and found that the semicrystalline nature of P3HT limits the HSP prediction.<sup>25</sup> Zhao *et al.* used different HSP values to differentiate the cohesive interaction to solvents between

Nanoscale Page 10 of 47

backbone and sidechain and found that the backbone has more polarity and dispersion attributions than alkyl sidechains. However, HSP values are empirical and this measurement requires several grams of materials and is often time-consuming. On the other hand, static light scattering (SLS) can be used to probe solvent quality in dilute solution, which only requires little samples and is easily accessible compared to small-angle neutron and X-ray scattering. Recently Liu *et al.* studied the effect of solvent quality on the aggregate shape of DPP-DTT in chloroform. A negative second virial coefficient (-4.4~+0.5\*10<sup>-6</sup> ml<sup>3</sup>\*mol/g<sup>2</sup>) is obtained which indicates chloroform is a bad solvent despite that DPP-DTT can disperse into chloroform. Bin *et al.* measured fractal dimensions of poly(9,9-dioctylfluorene) (PFO) chain solution in chlorobenzene, toluene, tetrahydrofuran, and chloroform. PFO forms aggregates in all solvents at concentrations above 1.0 mg/ml despite various aromaticity. Li *et al.* investigated the effect of chloroform/toluene on the bulky polydiarylfluorene (P7DPF) solution. By using SLS, the fractal dimensions of the aggregates increase from 0.62 to 1.76 as poor solvent toluene volume fraction increases from 0.5 to 1.0. However, what is the solvent quality for other CPs and how does the solvent quality impact the chain conformation is not well known.

In this work, we studied a series of thiophene-derived model CPs in various solvents. These CPs include poly(3-alkylthiophenes) (P3ATs) with various sidechain lengths, ranging from -C<sub>4</sub>H<sub>9</sub> to -C<sub>12</sub>H<sub>25</sub> (P3BT to P3DDT), PQT-12 and PBTTT-12, and thiophene-derived donor-accepter CP PffBT4T-C9C13. We performed dynamics light scattering (DLS), static light scattering (SLS), UV-Vis, and small angle X-ray scattering (SAXS). The second virial coefficient  $(A_2)$  can be obtained by constructing a Debye plot from the SLS experiment. We found that chlorobenzene is a better solvent than toluene and chloroform towards various CPs, where all CPs in chlorobenzene showed a positive  $A_2$ . For P3ATs in non-polar solvents like toluene, a longer alkyl sidechain promotes better polymer-solvent interaction towards non-polar solvents and sidechain and thus higher A<sub>2</sub>. Meanwhile, PQT-12 and PBTTT-12, have a stronger tendency to aggregate in all the solvents, with a much smaller negative  $A_2$ . A donor-acceptor CP, PffBT4T-C9C13 in chlorobenzene also has a negative  $A_2$  of -2.8\*10<sup>-6</sup> cm<sup>3</sup>\*mol/g<sup>2</sup> even at an elevated measurement temperature of 65°C. We performed coarse-grained molecular dynamics (CG-MD) simulation on CPs with various architectures and grafting density in an implicit solvent with various solvent qualities, and our simulation results suggest that CPs with dense and branched sidechains have better polymer-solvent interaction. Our work here provides insights into the solution behavior of Page 11 of 47 Nanoscale

conjugated polymers that can guide both the design and process of CPs toward next-generation organic electronics.

#### 3 Experiment

#### 3.1 Materials

All P3ATs (Rieke metals), PQT-12 (Sigma-Aldrich), PBTTT-12 (Sigma-Aldrich), and PffBT4T-C9C13 (Ossila,  $M_{\rm w}=123{\rm kDa}$ ) were used as received. All the solvents (toluene, chlorobenzene, tetrahydrofuran, and chloroform) were purchased from Sigma-Aldrich and filtered through a 0.2  $\mu$ m PTFE filter before use. CPs were first dissolved at 80°C in various solvents overnight for better dispersion, then cooled down to measurement temperature for the test.

#### 3.2 UV-Vis

UV-Vis spectroscopy was performed on a Cary 5000 UV-Vis-NIR spectrophotometer (Agilent Technologies) with a 3 mm optical path quartz cuvette.

#### 3.3 Dynamic light scattering (DLS) and static light scattering (SLS)

Dynamic light scattering and static light scattering were performed on a Brookhaven BI-200SM research goniometer with BI-APD avalanche photodiode detector and 35mW 633nm laser source with 90°-angle geometry. Solutions were held in a capped glass tube and the temperature was controlled by a cyclic intracooler with a temperature variation of  $\pm 1$ °C.

In DLS, an autocorrelation function, C(t) is calculated based on the fluctuation signal:

$$C(t) = Ae^{-2\Gamma t} + B$$

wherein A is the optical constant through instrument design,  $\Gamma$  is the relaxation of the fluctuation, t is time and B is the constant background.  $\Gamma$  and q are defined as  $\Gamma = Dq^2$  and scattering vector  $q = \frac{4\pi n_0}{\lambda_0} sin(\frac{\theta}{2})$ . The size distribution of the particles was analyzed by the Brookhaven software using cumulants analysis.

In SLS, the Debye plot was constructed based on static scattering intensity:

$$\frac{Hc}{R(q)} = \frac{1}{M_w} \left( 1 + \frac{1}{3} q^2 R_g^2 + \dots \right) + 2A_2 c$$

Nanoscale Page 12 of 47

Where 
$$H = \frac{4\pi^2}{N_A \lambda^4} n^2 \left(\frac{dn}{dc}\right)^2$$
, and  $R(q) = \frac{I_s(\theta)r^2}{I_0 V_s(\theta)} = \frac{I_{solution}/I_{0,solution} - I_{solvent}/I_{0,solvent}}{I_{std}/I_{0,std}} R_{std}$ . The

differential refractive index,  $\frac{dn}{dc}$ , are measured and listed in supplementary information under **Table S3.** 

#### 3.4 Small-angle X-ray Scattering (SAXS)

SAXS experiments were performed at the NSLS-II 12-ID located at Brookhaven National Laboratory (BNL). Polymers were dissolved in toluene or chlorobenzene at a concentration of 8 mg\*ml $^{-1}$ . The solution was sealed in a thin-wall capillary tube with a tube diameter of 1 mm. 16.1 keV X-ray was used to minimize the absorption from chlorinated solvents and two sample-to-detector distances were used to cover the range of scattering wavevector q from 0.01 to 3.0 Å $^{-1}$ . The solution temperature was controlled by Lake Shore Cryotronics with an accuracy of  $\pm 1^{\circ}$ C. Background scattering was subtracted carefully in Igor WaveMetrics along with the Nika package. The model fitting was done in SasView 5.0 software.

#### 3.5 CG-MD simulations

We employed generic bead-spring CG models of CPs and MD simulations to systematically explore the conformational behaviors of CPs chain in dilute solutions. We model CPs based on various branched chain structures as depicted in **Figure 4a**, aiming to represent a broad range of CPs. Specifically, the CG model comprises a linear backbone composed of  $N_{\rm bb}$  monomers, represented by cyan beads. The key feature of our CG model lies in the diverse sidechain architectures (orange beads) appended to this backbone, enabling a systematic examination of the impact of different sidechain arrangements on the conformational behavior of the polymer. In this study, all physical quantities within our system are expressed in reduced Lennard-Jones (LJ) units. These units include  $\varepsilon$ ,  $\sigma$ , and m for energy, length, and mass, respectively. Additionally, time, temperature, and pressure are defined by  $\tau$ ,  $\varepsilon/k_{\rm B}$ , and  $\varepsilon/\sigma^3$ , respectively, where  $\tau = \sqrt{m\sigma^2/\varepsilon}$  with  $k_{\rm B}$  representing the Boltzmann constant. Importantly, these reduced units are amenable to straightforward conversion into the physical units applicable to real-world laboratory measurements of polymer materials. Similar models have been widely harnessed to investigate a broad spectrum of dynamic, conformational, structural, and mechanical properties exhibited by CPs, both in melt and solution states.<sup>30</sup>

Page 13 of 47 Nanoscale

Significantly, to account for polymer-solvent interactions, we have introduced a dimensionless parameter denoted as  $\lambda$ , which serves as a valuable tool for qualitatively capturing the varying quality of the solvent in a solution state. By adjusting the parameter  $\lambda$  across particles, we can effectively modulate the 'solvent quality'. Specifically, when  $\lambda$  is set to 0, the polymer should be in an ideal good solvent, characterized by purely repulsive interactions. However, as we incrementally increase the value of  $\lambda$ , we could systematically decrease in solvent quality, attributable to the introduction of attractive forces among the polymer chain (see ref<sup>31</sup> for a detailed study of the relationship between solvent quality and parameter  $\lambda$ ).

#### 4 Result and discussion

First, we studied solvent and polymer interactions for polythiophenes with different lengths of sidechain, ranging from -C<sub>4</sub>H<sub>9</sub> to C<sub>12</sub>H<sub>25</sub> (Figure 1a). Two commonly used solvents, chlorobenzene (CB) and toluene (Tol) were studied here. Upon heating all the P3ATs form clear bright orange solutions. When cooled down to 20°C, all absorption spectra for polythiophenes (Figure 1b, c and Figure S1) are similar. However, P3BT, PQT-12, and PBTTT-12 solutions become darker upon cooling in both CB and Tol, with an absorption tail above 600 nm, which interacts with the He-Ne laser. This is typically referred to as the absorption of aggregates where the backbone is stacked closer<sup>32</sup> and this aggregation is further confirmed by DLS. The delayed autocorrelation function decay is caused by the slow Brownian motion of large objects and the particle size is converted by the Stokes-Einstein equation (Figure 1d-g). The peak at around 10 nm in diameter comes from the random Brownian motion of the dissolved single chain. However, P3BT, PQT-12, and PBTTT-12 solutions showed extra peaks larger than 100 nm in the histogram of particle size (Figure 1d, g and Figure S2), indicating the existence of large multi-chain aggregates. This strong aggregation tendency is expected as P3BT has the shortest sidechain (- $C_4H_9$ ) and PQT-12 and PBTTT-12 have better charger device performance,<sup>33</sup> where close  $\pi$ - $\pi$ stacking overwhelmed entropy-favored dissolving processing due to insufficient sidechain length and reducing sidechain graft density.

**Table 1** Summary of molar mass and sidechain mass fraction of CPs.

Name	Alkyl sidechain	$M_{ m w}$ (avg) kg/mol	Dispersity D	Sidechain mass fraction $m_{\rm f}$	Regioregularity
P3BT	-C4H9	<del>60k</del> 41k	2.3	0.41	85%

P3HT	-C6H13	60k <u>42k</u>	<u>2.0</u>	0.51	90%
P3OT	-C8H17	80k <u>60k</u>	<u>2.0</u>	0.58	92%
P3DT	-C10H21	80k <u>62k</u>	<u>2.1</u>	0.64	92%
P3DDT	-C12H25	60k	<u>2.0</u>	0.68	92%
PQT-12	-C12H25	17.5k	<u>3.0~3</u>	0.51	
PBTTT-12	-C12H25	<del>50k</del> <u>60k</u>	<u>3.0</u>	0.53	

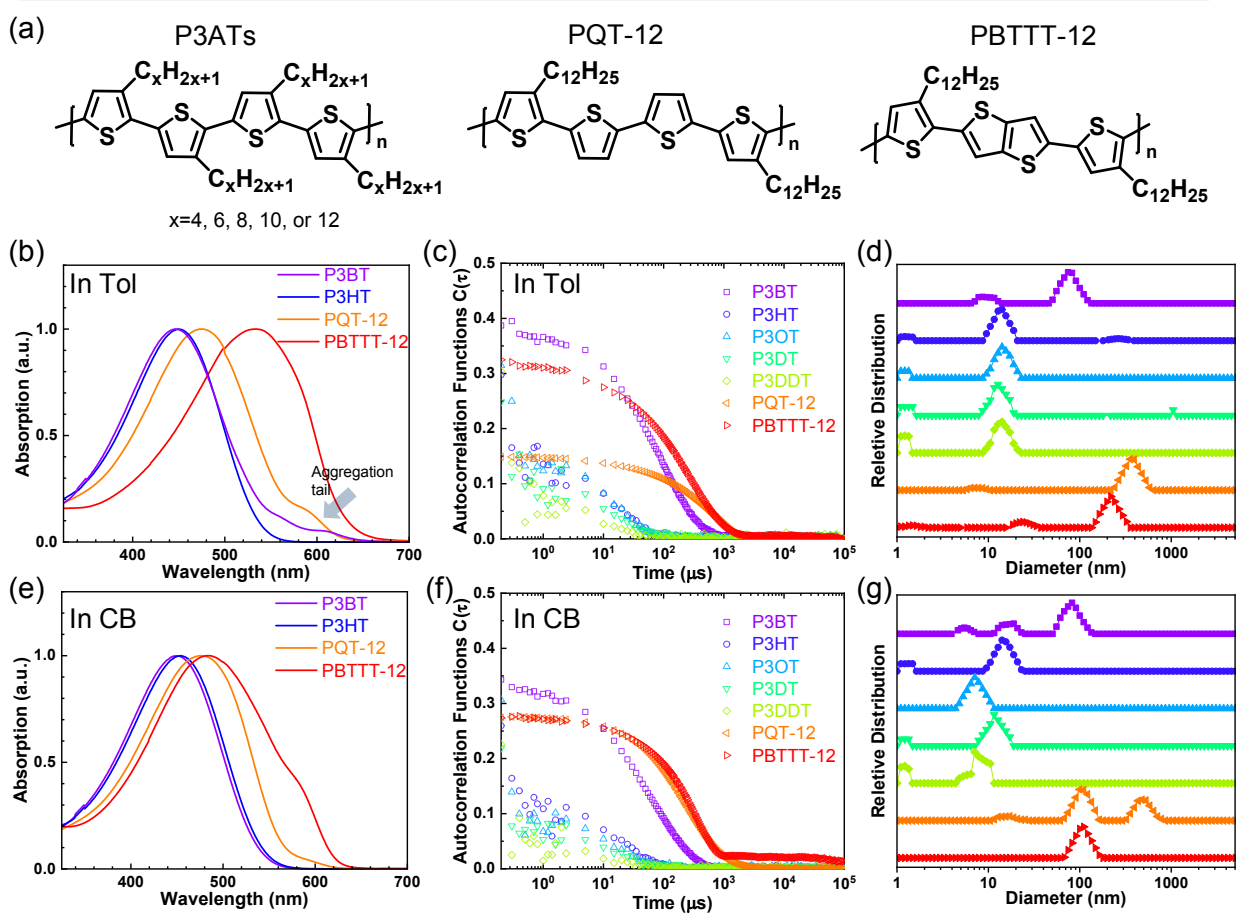


**Figure 1** (a) Chemical structure of P3ATs, PQT-12 and PBTTT-12. The UV-Vis absorption spectrum of CPs in toluene (b) and CB (e) at 20°C. Autocorrelation curve of CPs in toluene (c) and CB (f) from DLS measurement at 20°C. (e) Size distribution of CPs in toluene (d) and CB (g) from DLS testmeasurement.

Page 15 of 47 Nanoscale

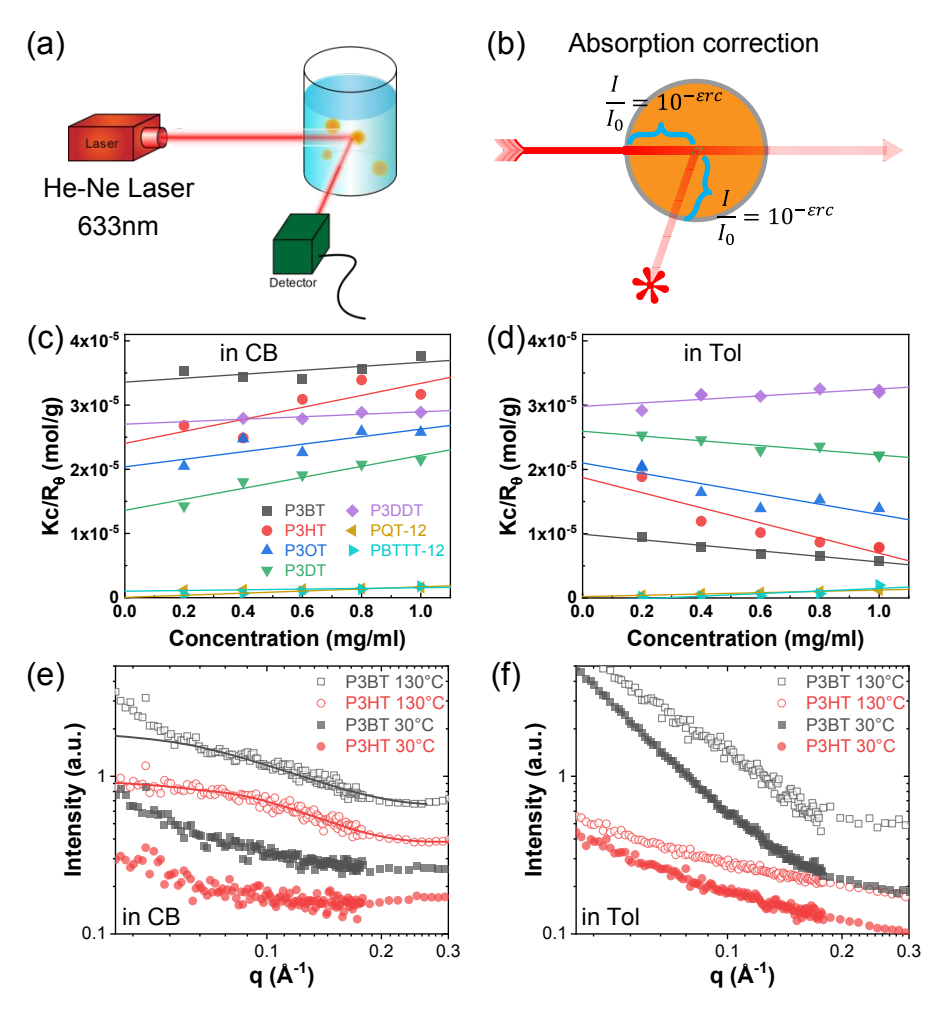


**Figure 2** (a) An illustration of the setup of static light scattering. (b) The principle of absorption correction is based on the Lambert-Beer law. (c, d) Debye plot of CPs in CB (c) and in toluene(d) at 20°C. Absorption correction was applied to PQT-12, PBTTT-12 in CB and P3BT, PQT-12, and PBTTT-12 in Tol. (e, f) SAXS result of P3BT and P3HT in CB (e) and Tol (f) at 30°C (closed symbol) and 130°C (open symbol). Continuous lines are fitting curves using a flexible cylinder model and the scattering profile is shifted vertically for clarity.

Then, we performed SLS on dilute solutions of CPs with the concentration ranging from 0.2 to 1.0 mg/ml. The SLS setup is illustrated in **Figure 2a**, where the light scattering intensity of different concentration solutions is measured by a photon detector with a 633 nm wavelength filter. Some CPs solutions could absorb red light, which could lower the scattering intensity at different angles and cause issues to constructing Debye plot. Thus, proper absorption correction for those samples is needed, where Lambert-Beer law was used. The light path is illustrated in **Figure 2b** 

Page 16 of 47

Nanoscale

and the Debye plot was plotted in **Figure 2c**, **d** and **Figure S7**. The linear fit yields from the data point in the Debye plot give  $A_2$ , half of the slope, which is listed in

**Table 2.** We found that CB is a better solvent for all P3ATs compared to toluene, THF, and chloroform, as all A<sub>2</sub> in CB are positive but some negative in other solvents. As the sidechain length increases, the A<sub>2</sub> in toluene and THF increases, which indicates better polymer-solvent interaction. This is expected as the sidechain volume mass fraction increases (**Table 1**) as sidechain length increases which is more soluble than the rigid backbone of CPs based on HSP theory (**Figure S6** and **Table S4**). To investigate the impact of sidechain length on solvent quality, we conducted Small-Angle X-ray Scattering (SAXS) analysis to examine the chain conformation of both P3BT and P3HT in CB and Tol. The scattering profiles are depicted in **Figure 2e** for CB solution and **Figure 2f** for Tol solution. It is evident that both polymers form homogenous solutions in both solvents. When the temperature was set at 30°C in CB, the scattering intensity of both polymers increased in the low-q region, indicating the presence of loose aggregates with a large feature size. At elevated temperatures (130°C), a Guinier region emerged in the intermediate q range. Notably, the low-q upturn of intensity was observed in P3BT but not in P3HT, suggesting a more effective dissolution of P3HT with longer sidechains. Fitting the curve using the flexible cylinder model allowed us to probe the chain conformation, and the results are detailed in

Table 3. The polymer chain conformation aligns well with that of a flexible cylinder, exhibiting a cylinder radius of 1.2±0.4nm for P3BT and 1.3±0.2nm for P3HT, indicative of a well-dissolved single chain. In contrast, toluene could only disperse both polymers, since the evidence of single chain scattering or an obvious Guinier plateau regional is missing.<sup>34</sup> This aligns with the solvent quality assessment, affirming that CB serves as a better solubilizing solvent for P3ATs when compared to toluene. Furthermore, the solvent quality can impact the macroscopic spectroscopy, as shown in **Figure S4**. For those dispersed aggregate, the polymer exhibits a redshifted absorption peak at around 610nm, in additional to the primary absorption at 450nm for P3BT in toluene.

However, sidechain architecture also played a role as we compared P3HT, PQT-12, and PBTTT-12, where the sidechain volume-mass fraction is similar as calculated in Table 1. PQT-12 and PBTTT-12 strongly aggregate and form light-absorbing solutions especially in THF and chloroform, so we only measured  $A_2$  for CPs in CB and toluene. The positive  $A_2$  of PQT-12 and PBTTT-12 is not an indication of a fully dissolved single chain in the solution as this could be

Page 17 of 47 Nanoscale

achieved by a dedicated self-assembled structure where the sidechain is exposed outside while the backbone is buried inside. This is not surprising as CPs have complex multi-length scale structures in the solution. This is not surprising as CPs have complex multi-length scale structures in the solution. The double-length sidechain chain and reduced sidechain grafting density lead to a strong aggregate attendance in all the solvents. This strong aggregation tendency is expected for semicrystalline CPs where PQT-12 and PBTTT-12 are more crystalline in the solid state revealed by DSC (**Figure S8**). The negative  $A_2$  of P3HT in toluene suggests bad polymer-solvent interaction, indicating polymer intrachain collapse and interchain aggregation are thermodynamically favorable. This slow and subtle transition can be observed in aging tests over days by DLS (**Figure S9**) and a similar effect has been reported previously  $^{13}$ ,  $^{36}$ . After cooling down from the hot solution and aging at room temperature, the hydrodynamic diameter of the particle keeps increasing in the P3HT toluene solution but is maintained in the CB solution. Thus, we conclude that CB is the best solvent for all the P3ATs compared to Tol, THF, and chloroform.

**Table 2** A<sub>2</sub> value of CPs in all the solvents at 20°C.

Dalyman Calyant		$A_2 (\times 10^{-3} \text{ c})$	$cm^3*mol/g^2$	
Polymer\Solvent —	СВ	Toluene	THF	Chloroform
P3BT	1.5	-2.2	-7.8	-4.6
P3HT	4.7	-5.9	-4.4	-3.5
P3OT	2.9	-4.0	-3.2	-4.7
P3DT	4.3	-1.9	-1.5	-2.6
P3DDT	1.0	1.4	-3.8	-4.8
PQT-12	0.3	0.5	none	none
PBTTT-12	0.8	-0.5	none	none

**Table 3** Fitting parameters from SAXS on P3BT and P3HT using a flexible cylinder model.

Name	Length/nm	Kuhn length/nm	Radius/nm	Fitting error $\chi^2$
P3BT in CB 130°C	5.3±0.5	5.8±0.6	1.2±0.4	0.22
P3HT in CB 130°C	$3.2 \pm 0.6$	$4.6 \pm 0.8$	$1.3\pm0.2$	0.15

We then examined sidechain architecture's effect on solvent quality by comparing P3HT, PQT-12, and PBTTT-12. They have similar sidechain fractions but different sidechain lengths, grafting density, and backbone stiffness. PQT-12 and PBTTT-12 strongly aggregate in the solution at room temperature and form a deep red solution (**Figure S1**). The aggregate size is larger than

Nanoscale Page 18 of 47

100nm in diameter as seen by DLS in dilute solution (**Figure 1d** and **g**), while the aggregate could be long fiber as seen previously<sup>37</sup>. This makes both DLS and SLS harder as the solution strongly absorbs the red light and the thermal lens effect distorts the optical light path<sup>38</sup>. This leads to a significant broadening of beam path and distorted transmission beam as shown in **Figure S10**. Nonetheless, P3HT has better polymer-solvent interaction than its analog PQT-12 and PBTTT-12, with different sidechain architecture.

Page 19 of 47 Nanoscale

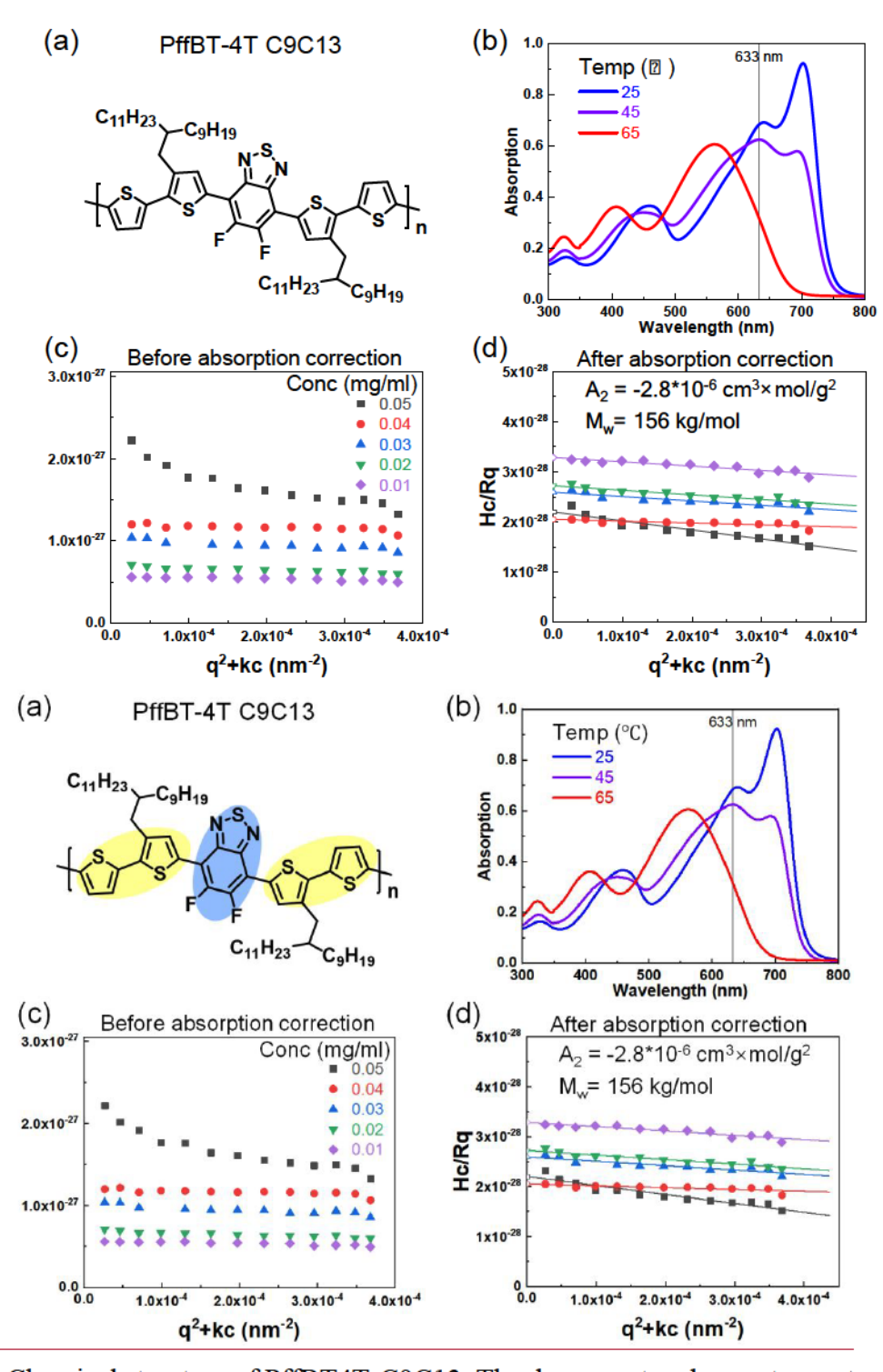


**Figure 3** (a) Chemical structure of PffBT4T-C9C13. The donor part and acceptor part are colored as yellow and blue units, respectively. (b) UV-Vis of PffBT4T-C9C13 in CB at various temperatures. The laser wavelength used in the light scattering test is marked in a gray line. (c, d) SLS of PffBT4T-C9C13 in CB at 65°C before and after absorption correction, respectively.

Nanoscale Page 20 of 47

To explore high-performance CPs, we also examined a donor-acceptor CPs PffBT4T-C9C13 in a solvent chlorobenzene. PffBT4T-C9C13 has significant temperature-dependent absorption (Figure 3b) and aggregation behavior in the solution that has been well-reported.<sup>39</sup> Large aggregates form immediately as the solution cools down and breaks apart gradually at elevated temperatures. The solution optical absorption at 633nm decreases, making SLS possible to probe the solvent quality at a single chain level. Before light absorption correction, the Zimm plot was not meaningful since it gives a negative molar mass. After the light absorption correction, we got  $M_{\rm w}$ =156 kg/mol, which is comparable to the GPC result ( $M_{\rm w, GPC}$ =123 kg/mol). Interestingly, the  $A_2$ =-2.8\*10<sup>-6</sup> cm<sup>3</sup>\*mol/g<sup>2</sup>, which is on the similar magnitude of DPPT in chloroform.<sup>27</sup> This small and negative  $A_2$  showed that CPs have thermodynamically unfavorable polymer-solvent interaction where aggregation is inevitable. However, one  $A_2$  parameter cannot differentiate the interaction between the sidechain and backbone to the solvent, furthermore, there is a lack of synthetically achievable variations of the sidechain. Overall, the complex CPs structure with rigid conjugated backbone and flexible sidechain, heterogeneous dynamics between backbone and sidechains, and particularly strong  $\pi$ - $\pi$  interaction between backbone lead to peculiar self-assembly behavior of CPs in the solution.

Page 21 of 47 Nanoscale

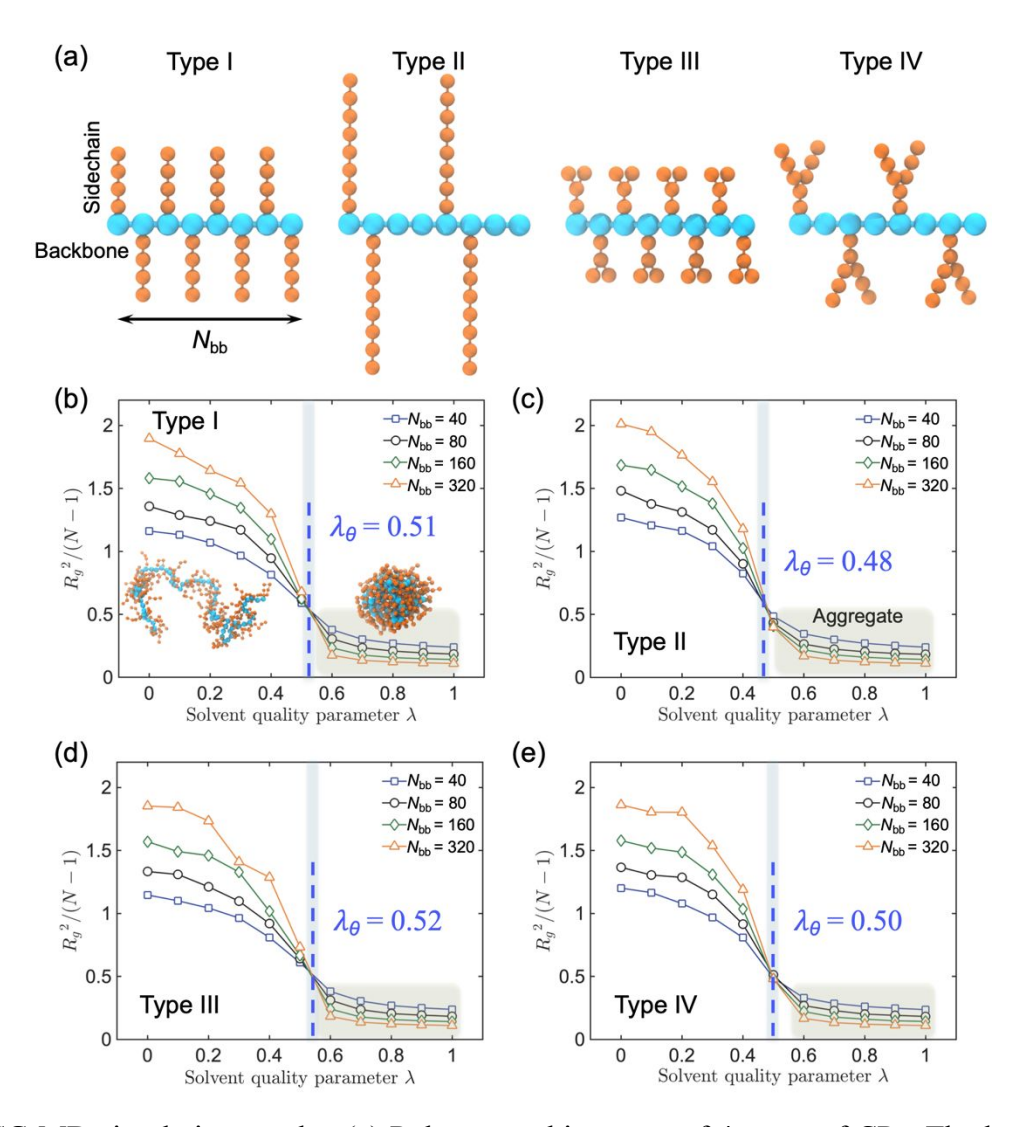


**Figure 4** CG MD simulation results. (a) Polymer architectures of 4 types of CPs. The backbone and sidechain are represented as beads P1 and P2, respectively. (b-e) Reduced  $R_g$  of polymer chain as a function of solvent quality parameter  $\lambda$  for type I to IV, respectively. A lower value of  $\lambda$  corresponds to better solvent quality. The location of the  $\theta$  point is indicated by the blue dashed line.

To elucidate the impact of solvent quality and sidechain architecture on CPs in a broader context, we conducted CG-MD simulations to explore four distinct sidechain architectures of CPs representing diverse chemical structures, as shown in **Figure 4a**. Specifically, we constructed CPs with (I) short dense sidechains, (II) long and less dense sidechains, (III) dense branched sidechains, and (IV) less dense branched sidechains, respectively. The introduction of the solvent quality parameter  $\lambda$  to characterize polymer-solvent interactions provides a versatile means to fine-tune

Nanoscale Page 22 of 47

solvent quality by adjusting  $\lambda$  among individual particles, where higher  $\lambda$  values correspond to poor solvent quality. In our simulations, we systematically track polymer chain conformational changes and record the time-dependent evolution of the radius of gyration ( $R_g$ ) under varying solvent conditions, while also accounting for the influence of sidechain architecture, as shown in **Figure 4**.

Herein, we consistently observe three distinct stages across all scenarios. For  $\lambda$  values below 0.4, the polymer chain exhibits its largest  $R_{\rm g}$ , indicative of an extended coil conformation, as exemplified in the illustrative representation in Figure 4b. This behavior aligns with the expected characteristics of a chain in a favorable solvent environment. As  $\lambda$  progressively increases,  $R_{\rm g}$ gradually diminishes, reflecting a gradual compaction of the polymer coil within the solution consistent with the behavior of a fully dissolved chain. Conversely, when  $\lambda$  exceeds 0.6,  $R_g$  reaches a near minimum, signaling the collapse of the polymer chain into a compact single conformation, as demonstrated in the illustrative representation. Notably, as  $\lambda$  transitions from 0.4 to 0.6,  $R_{\rm g}$ experiences a rapid decrease, highlighting a notable phase transition that becomes increasingly well-defined with increasing chain length  $N_{\rm bb}$ . Moreover, four distinct polymer chains with different sidechain architectures are simulated to extrapolate  $\theta$  condition to quantitively compare solvent quality and chain conformation. When the polymer chain is in  $\theta$  state, polymer chains are free to coil and extend in solution which can be described by a random walk in 3D space, where the normalized coil size  $R_g^2/(N-1)$  is independent of polymer chain length N. Thus, we can find the  $\theta$  point with the intersection of four chains of different lengths in the  $\lambda$  coordinate. The larger the  $\lambda_{\theta}$ , the worse the solvent where the polymer chain can form a free coil, and thus this polymer is more soluble at a given solvent quality parameter  $\lambda$ . Hence, we conclude that Type III exhibits the most favorable solvent quality, owing to its higher density and branched configuration of sidechains.

We further explored other analogs of Type II and III, Type V and VI (**Figure S11**), wherein slight variations were introduced in terms of sidechain distribution along the backbone and sidechain branching position. However, our observations did not reveal any notable distinctions in  $\lambda_{\theta}$  between Type II and V, Type III and VI. These findings suggest that the process of CPs dissolution is primarily governed by entropy considerations, with a greater emphasis on the quantity of sidechain ends proving to be more influential in this context.<sup>40</sup> A parallel trend is also evident at higher temperatures, wherein polymer chains characterized by longer, denser, and more

Page 23 of 47 Nanoscale

extensively branched sidechains exhibit enhanced solubility, as shown in **Figure S12**. Consistent with the trends observed for  $R_g$ , we discerned a parallel pattern in response to variations in solvent quality for both the persistence length  $(L_p)$ , which quantifies chain rigidity and the end-to-end distance  $(R_{ee})$ , a parameter commonly used to characterize polymer chain conformational bends, as depicted in **Figure S13** and **Figure S14**, respectively.

To gain a deeper insight into the molecular-level shape of the polymer chain under various solvent conditions, we further examine the shape descriptor known as relative shape anisotropy  $\kappa^2$ , which describes the degree of anisotropy in the chain's shape, specifically regarding its tendency toward rod-like ( $\kappa^2 = 1$ ), planar symmetric ( $\kappa^2 = 0.25$ ), or spherical configurations ( $\kappa^2 = 0.4$ ). As shown in **Figure S15**,  $\kappa^2$  exhibits fluctuations within the range of 0.1 to 0.2, remaining relatively stable in a good solvent ( $0 < \lambda < 0.4$ ) across all six types of polymer chains. This stability suggests some level of elongation or asymmetry in molecular structure, with minimal influence from sidechain architecture. Conversely, as the solvent quality deteriorates ( $0.6 < \lambda < 1.0$ ),  $\kappa^2$  decreases significantly towards zero, signaling the onset of polymer chain aggregation.

#### 5 Conclusion

To conclude, we measured the second virial coefficient  $A_2$  by static light scattering to quantify solvent quality on a series of CPs solutions and investigated the effects of sidechain volume fraction, sidechain architecture, and backbone architecture on optical absorption, particle size, and chain conformation in solution state. We studied (1) P3ATs with various sidechain lengths, from C4 to C12, (2) two P3HT's analogous PQT-12 and PBTTT-12, and (3) PffBT4T-C9C13, in a variety of solvents. We found that chlorobenzene is a better solvent than toluene and chloroform towards various CPs, where more CPs have positive  $A_2$  in CB only. For P3ATs in non-polar solvents like toluene, longer sidechain promotes better polymer-solvent interaction towards alkyl sidechains and thus higher  $A_2$ . Besides sidechain fraction, sidechain architecture also impacts the aggregation tendency. For example, PQT-12 and PBTTT-12 have a stronger tendency to aggregate in all the solvents, despite having a similar sidechain volume ratio to P3HT. Meanwhile, backbone architecture also influences the solvent quality and aggregation tendency. A donor-acceptor CP, PffBT4T-C9C13 in CB also has a negative  $A_2$  at 65°C. We performed CG molecular dynamics simulation on CPs with various backbone and sidechain architectures in an implicit solvent with various solvent qualities, which suggests that CPs with dense and branched sidechains have

Nanoscale Page 24 of 47

stronger polymer-solvent interaction and better solubility. Overall, our study provides quantitative insight into the design and processing of CPs from a polymer-solvent interaction perspective.

#### ASSOCIATED CONTENT

#### **Supporting Information**

The following information are provided in the supporting information. They are available free of charge. Sample preparation, dn/dc measurement, HSP calculation, DSC measurements, scattering and spectroscopy measurements of the samples in solution and solid states. Additional coarse grain modelling data is included as well.

#### **Corresponding Author**

Xiaodan Gu, Correspondence to: Xiaodan Gu (Email: xiaodan.gu@usm.edu)

#### **Author Contributions**

X.G. and L.F. conceived and directed the project. All experiments were done and analyzed by G.M. Simulation was performed by Z.L under the guidance of W.X. The manuscript was written by G.M. with everyone's input. All authors have revised and approved the final version of the manuscript.

#### **Funding Sources**

U.S. National Science Foundation (NSF) under award number of 2003733, 2004133, 2304968 and 2304969

#### **Notes**

The authors declare no competing financial interest.

#### Acknowledgements

This work was financially supported by the U.S. National Science Foundation (NSF) under award number of 2003733, 2004133, 2304968 and 2304969. Z.L. and W.X. acknowledged the support from NSF Award No. CMMI-2237063. We thank BNL beamline scientists Wasik Patryk

Page 25 of 47 Nanoscale

and Guillaume Freychet for their help during the SAXS measurement. This research used resources 12-ID of the National Synchrotron Light Source II, a U.S. Department of Energy (DOE) Office of Science User Facility operated for the DOE Office of Science by Brookhaven National Laboratory under Contract No. DE-SC0012704.

Page 26 of 47

#### 6 References

- (1) Zeng, R.; Zhu, L.; Zhang, M.; Zhong, W.; Zhou, G.; Zhuang, J.; Hao, T.; Zhou, Z.; Zhou, L.; Hartmann, N.; et al. All-polymer organic solar cells with nano-to-micron hierarchical morphology and large light receiving angle. *Nat Commun* **2023**, *14* (1), 4148. DOI: 10.1038/s41467-023-39832-4. Zhu, L.; Zhang, M.; Xu, J.; Li, C.; Yan, J.; Zhou, G.; Zhong, W.; Hao, T.; Song, J.; Xue, X.; et al. Single-junction organic solar cells with over 19% efficiency enabled by a refined double-fibril network morphology. *Nat Mater* **2022**, *21* (6), 656-663. DOI: 10.1038/s41563-022-01244-y.
- (2) Rivnay, J.; Inal, S.; Salleo, A.; Owens, R. M.; Berggren, M.; Malliaras, G. G. Organic electrochemical transistors. *Nat. Rev. Mater.* **2018**, *3* (2). DOI: 10.1038/natrevmats.2017.86. (3) Yu, X.; Chen, L.; Li, C.; Gao, C.; Xue, X.; Zhang, X.; Zhang, G.; Zhang, D. Intrinsically Stretchable Polymer Semiconductors with Good Ductility and High Charge Mobility through Reducing the Central Symmetry of the Conjugated Backbone Units. *Adv Mater* **2023**, *35* (17), e2209896. DOI: 10.1002/adma.202209896. Ibanez, J. G.; Rincon, M. E.; Gutierrez-Granados, S.; Chahma, M.; Jaramillo-Quintero, O. A.; Frontana-Uribe, B. A. Conducting Polymers in the Fields of Energy, Environmental Remediation, and Chemical-Chiral Sensors. *Chem Rev* **2018**, *118* (9), 4731-4816. DOI: 10.1021/acs.chemrev.7b00482.
- (4) Reynolds, J. R.; Thompson, B. C.; Skotheim, T. A. *Conjugated Polymers: Properties, Processing, and Applications*; CRC press, 2019. DOI: 10.1201/9780429190520.
- (5) Kukhta, N. A.; Luscombe, C. K. Gaining control over conjugated polymer morphology to improve the performance of organic electronics. *Chem Commun (Camb)* **2022**, *58* (50), 6982-6997. DOI: 10.1039/d2cc01430k.
- (6) Swager, T. M. 50th Anniversary Perspective: Conducting/Semiconducting Conjugated Polymers. A Personal Perspective on the Past and the Future. *Macromolecules* **2017**, *50* (13), 4867-4886. DOI: 10.1021/acs.macromol.7b00582.
- (7) Xu, Y. C.; Ding, L.; Yao, Z. F.; Shao, Y.; Wang, J. Y.; Zhang, W. B.; Pei, J. Conjugated Polymers in Solution: A Physical Perspective. *J Phys Chem Lett* **2023**, *14* (4), 927-939. DOI: 10.1021/acs.jpclett.2c03600.
- (8) Ma, G. R.; Leng, M. W.; Li, S.; Cao, Z. Q.; Cao, Y. R.; Tabor, D. P.; Fang, L.; Gu, X. D. Robust chain aggregation of low-entropy rigid ladder polymers in solution. *J. Mater. Chem. C* **2022**, *10* (37), 13896-13904. DOI: 10.1039/d2tc00761d.
- (9) Wang, D. P.; Yuan, Y.; Mardiyati, Y.; Bubeck, C.; Koynov, K. From Single Chains to Aggregates, How Conjugated Polymers Behave in Dilute Solutions. *Macromolecules* **2013**, *46* (15), 6217-6224. DOI: 10.1021/ma4011523.
- (10) Wu, Y.; Ding, Z. C.; Zhang, Q.; Liang, X.; Yang, H.; Huang, W. L.; Su, Y. L.; Zhang, Y.; Hu, H. L.; Han, Y. C.; et al. Increasing H-Aggregates via Sequential Aggregation to Enhance the Hole Mobility of Printed Conjugated Polymer Films. *Macromolecules* **2022**, *55* (19), 8609-8618. DOI: 10.1021/acs.macromol.2c01701. Traiphol, R.; Charoenthai, N.; Srikhirin, T.; Kerdeharoen, T.; Osotchan, T.; Maturos, T. Chain organization and photophysics of conjugated polymer in poor solvents: Aggregates, agglomerates and collapsed coils. *Polymer* **2007**, *48* (3), 813-826. DOI: 10.1016/j.polymer.2006.12.003. Li, Y. C.; Chen, K. B.; Chen, H. L.; Hsu, C. S.; Tsao, C. S.; Chen, J. H.; Chen, S. A. Fractal aggregates of conjugated polymer in solution state. *Langmuir* **2006**, *22* (26), 11009-11015. DOI: 10.1021/la0612769.
- (11) Xi, Y.; Wolf, C. M.; Pozzo, L. D. Self-assembly of donor-acceptor conjugated polymers induced by miscible 'poor' solvents. *Soft Matter* **2019**, *15* (8), 1799-1812. DOI: 10.1039/c8sm02517g.

- (12) Nguyen, T. Q.; Doan, V.; Schwartz, B. J. Conjugated polymer aggregates in solution: Control of interchain interactions. *J. Chem. Phys.* **1999**, *110* (8), 4068-4078. DOI: 10.1063/1.478288.
- (13) Kleinhenz, N.; Rosu, C.; Chatterjee, S.; Chang, M.; Nayani, K.; Xue, Z. Z.; Kim, E.; Middlebrooks, J.; Russo, P. S.; Park, J. O.; et al. Liquid Crystalline Poly(3-hexylthiophene) Solutions Revisited: Role of Time-Dependent Self-Assembly. *Chem. Mater.* **2015**, *27* (7), 2687-2694. DOI: 10.1021/acs.chemmater.5b00635.
- (14) Li, Y. C.; Chen, C. Y.; Chang, Y. X.; Chuang, P. Y.; Chen, J. H.; Chen, H. L.; Hsu, C. S.; Ivanov, V. A.; Khalatur, P. G.; Chen, S. A. Scattering study of the conformational structure and aggregation behavior of a conjugated polymer solution. *Langmuir* **2009**, *25* (8), 4668-4677. DOI: 10.1021/la803339f. Schwartz, B. J. Conjugated polymers as molecular materials: how chain conformation and film morphology influence energy transfer and interchain interactions. *Annu Rev Phys Chem* **2003**, *54*, 141-172. DOI: 10.1146/annurev.physchem.54.011002.103811. Heffner, G. W.; Pearson, D. S.; Gettinger, C. L. Characterization of poly(3 octylthiophene). I: Molecular characterization in dilute solution. *Polymer Engineering & Science* **2004**, *35* (10), 860-867. DOI: 10.1002/pen.760351008.
- (15) Zhang, H.; Li, T.; Liu, B.; Ma, T. N.; Huang, L.; Bai, Z. M.; Lu, D. Effect and Mechanism of Solvent Properties on Solution Behavior and Films Condensed State Structure for the Semirigid Conjugated Polymers. *Chin. J. Polym. Sci.* **2021**, *39* (7), 796-814. DOI: 10.1007/s10118-021-2555-6. Moris, M.; Van den Eede, M. P.; Koeckelberghs, G.; Deschaume, O.; Bartic, C.; Clays, K.; Van Cleuvenbergen, S.; Verbiest, T. Solvent Role in the Self-Assembly of Poly(3-alkylthiophene): A Harmonic Light Scattering Study. *Macromolecules* **2021**, *54* (5), 2477-2484. DOI: 10.1021/acs.macromol.0c02544. Da Pian, M.; Maggini, M.; Vancso, G. J.; Causin, V.; Benetti, E. M. Assembly of poly-3-(hexylthiophene) nanocrystals in marginal solvent: The role of PCBM. *Eur. Polym. J.* **2018**, *109*, 222-228. DOI: 10.1016/j.eurpolymj.2018.09.049. Morgan, B.; Dadmun, M. D. The importance of solvent quality on the modification of conjugated polymer conformation and thermodynamics with illumination. *Soft Matter* **2017**, *13* (15), 2773-2780. DOI: 10.1039/c6sm02631a.
- (16) Li, J. K.; Shao, M. Y.; Yu, M.; Zhang, W.; Yang, Z. Y.; Yu, G.; Xu, J.; Cui, W. Revealing the Influences of Solvent Boiling Point and Alkyl Chains on the Adlayer Crystallinity of Furan-Diketopyrrole-Thienylene Copolymer at Molecular Level. *Langmuir* **2020**, *36* (1), 141-147. DOI: 10.1021/acs.langmuir.9b02604.
- (17) Opoku, H.; Nketia-Yawson, B.; Shin, E. S.; Noh, Y. Y. Organic field-effect transistors processed by an environmentally friendly non-halogenated solvent blend. *J. Mater. Chem. C* **2018**, *6* (3), 661-667. DOI: 10.1039/c7tc04823h. Jeon, G. G.; Lee, M.; Nam, J.; Park, W.; Yang, M.; Choi, J. H.; Yoon, D. K.; Lee, E.; Kim, B.; Kim, J. H. Simple Solvent Engineering for High-Mobility and Thermally Robust Conjugated Polymer Nanowire Field-Effect Transistors. *ACS Appl Mater Interfaces* **2018**, *10* (35), 29824-29830. DOI: 10.1021/acsami.8b07643. Keum, J. K.; Xiao, K.; Ivanov, I. N.; Hong, K. L.; Browning, J. F.; Smith, G. S.; Shao, M.; Littrell, K. C.; Rondinone, A. J.; Payzant, E. A.; et al. Solvent quality-induced nucleation and growth of parallelepiped nanorods in dilute poly(3-hexylthiophene) (P3HT) solution and the impact on the crystalline morphology of solution-cast thin film. *Crystengcomm* **2013**, *15* (6), 1114-1124. DOI: 10.1039/c2ce26666k. Scharsich, C.; Lohwasser, R. H.; Sommer, M.; Asawapirom, U.; Scherf, U.; Thelakkat, M.; Neher, D.; Köhler, A. Control of aggregate formation in poly(3-hexylthiophene) by solvent, molecular weight, and synthetic method. *J Polym Sci Pol Phys* **2012**, *50* (6), 442-453. DOI: 10.1002/polb.23022.

Nanoscale Page 28 of 47

- (18) Newbloom, G. M.; de la Iglesia, P.; Pozzo, L. D. Controlled gelation of poly(3-alkylthiophene)s in bulk and in thin-films using low volatility solvent/poor-solvent mixtures. *Soft Matter* **2014**, *10* (44), 8945-8954. DOI: 10.1039/c4sm00960f.
- (19) Chang, M.; Choi, D.; Fu, B.; Reichmanis, E. Solvent based hydrogen bonding: impact on poly(3-hexylthiophene) nanoscale morphology and charge transport characteristics. *ACS Nano* **2013**, 7 (6), 5402-5413. DOI: 10.1021/nn401323f.
- (20) Lee, W. Y.; Giri, G.; Diao, Y.; Tassone, C. J.; Matthews, J. R.; Sorensen, M. L.; Mannsfeld, S. C. B.; Chen, W. C.; Fong, H. H.; Tok, J. B. H.; et al. Effect of Non-Chlorinated Mixed Solvents on Charge Transport and Morphology of Solution-Processed Polymer Field-Effect Transistors. *Adv. Funct. Mater.* **2014**, *24* (23), 3524-3534. DOI: 10.1002/adfm.201303794.
- (21) Kwok, J. J.; Park, K. S.; Patel, B. B.; Dilmurat, R.; Beljonne, D.; Zuo, X. B.; Lee, B.; Diao, Y. Understanding Solution State Conformation and Aggregate Structure of Conjugated Polymers via Small Angle X-ray Scattering. *Macromolecules* **2022**, *55* (11), 4353-4366. DOI: 10.1021/acs.macromol.1c02449.
- (22) Hansen, C. M. Hansen solubility parameters: a user's handbook; CRC press, 2007. DOI: 10.1201/9781420006834.
- (23) Neu, J.; Samson, S.; Ding, K.; Rech, J. J.; Ade, H.; You, W. Oligo(ethylene glycol) Side Chain Architecture Enables Alcohol-Processable Conjugated Polymers for Organic Solar Cells. *Macromolecules* **2023**, *56* (5), 2092-2103. DOI: 10.1021/acs.macromol.2c02259. Emerson, J. A.; Toolan, D. T. W.; Howse, J. R.; Furst, E. M.; Epps, T. H. Determination of Solvent-Polymer and Polymer-Polymer Flory-Huggins Interaction Parameters for Poly(3-hexylthiophene) via Solvent Vapor Swelling. *Macromolecules* **2013**, *46* (16), 6533-6540. DOI: 10.1021/ma400597j. (24) Duong, D. T.; Walker, B.; Lin, J.; Kim, C.; Love, J.; Purushothaman, B.; Anthony, J. E.;
- Nguyen, T. Q. Molecular solubility and hansen solubility parameters for the analysis of phase separation in bulk heterojunctions. *J Polym Sci Pol Phys* **2012**, *50* (20), 1405-1413. DOI: 10.1002/polb.23153.
- (25) Machui, F.; Langner, S.; Zhu, X. D.; Abbott, S.; Brabec, C. J. Determination of the P3HT:PCBM solubility parameters via a binary solvent gradient method: Impact of solubility on the photovoltaic performance. *Sol. Energy Mater. Sol. Cells* **2012**, *100*, 138-146. DOI:
- 10.1016/j.solmat.2012.01.005. Machui, F.; Abbott, S.; Waller, D.; Koppe, M.; Brabec, C. J. Determination of Solubility Parameters for Organic Semiconductor Formulations. *Macromol. Chem. Phys.* **2011**, *212* (19), 2159-2165. DOI: 10.1002/macp.201100284.
- (26) Zhao, K. F.; Zhang, Q.; Chen, L.; Zhang, T.; Han, Y. C. Nucleation and Growth of P(NDI2OD-T2) Nanowires via Side Chain Ordering and Backbone Planarization. *Macromolecules* **2021**, *54* (5), 2143-2154. DOI: 10.1021/acs.macromol.0c02436.
- (27) Liu, C.; Hu, W. X.; Jiang, H. Q.; Liu, G. M.; Han, C. C.; Sirringhaus, H.; Boué, F.; Wang, D. J. Chain Conformation and Aggregation Structure Formation of a High Charge Mobility DPP-Based Donor-Acceptor Conjugated Polymer. *Macromolecules* **2020**, *53* (19), 8255-8266. DOI: 10.1021/acs.macromol.0c01646.
- (28) Liu, B.; Zhang, H.; Ren, J. X.; Ma, T. N.; Yu, M. N.; Xie, L. H.; Lu, D. Effect of solvent aromaticity on poly(9,9-dioctylfluorene) (PFO) chain solution behavior and film condensed state structure. *Polymer* **2019**, *185*. DOI: 10.1016/j.polymer.2019.121986.
- (29) Li, T.; Zhang, H.; Liu, B.; Ma, T. N.; Lin, J. Y.; Xie, L. H.; Lu, D. Effect of Solvent on the Solution State of Conjugated Polymer P7DPF Including Single-Chain to Aggregated State Structure Formation, Dynamic Evolution, and Related Mechanisms. *Macromolecules* **2020**, *53* (11), 4264-4273. DOI: 10.1021/acs.macromol.0c00579.

- (30) Wang, Y. F.; Zhang, S.; Freychet, G.; Li, Z. F.; Chen, K. L.; Liu, C. T.; Cao, Z. Q.; Chiu, Y. C.; Xia, W. J.; Gu, X. D. Highly Deformable Rigid Glassy Conjugated Polymeric Thin Films. Adv. Funct. Mater. 2023, n/a (n/a), 2306576. DOI: 10.1002/adfm.202306576. Zhao, H.; Shanahan, J. J.; Samson, S.; Li, Z.; Ma, G.; Prine, N.; Galuska, L.; Wang, Y.; Xia, W.; You, W.; et al. Manipulating Conjugated Polymer Backbone Dynamics through Controlled Thermal Cleavage of Alkyl Side Chains. Macromol Rapid Commun 2022, 43 (24), e2200533. DOI: 10.1002/marc.202200533. Cao, Z. Q.; Li, Z. F.; Zhang, S.; Galuska, L.; Li, T. Y.; Do, C.; Xia, W. J.; Hong, K. L.; Gu, X. D. Decoupling Poly(3-alkylthiophenes)' Backbone and Side-Chain Conformation by Selective Deuteration and Neutron Scattering. *Macromolecules* **2020**, *53* (24), 11142-11152. DOI: 10.1021/acs.macromol.0c02086. Zhang, S.; Alesadi, A.; Selivanova, M.; Cao, Z. Q.; Qian, Z. Y.; Luo, S. C.; Galuska, L.; Teh, C.; Ocheje, M. U.; Mason, G. T.; et al. Toward the Prediction and Control of Glass Transition Temperature for Donor-Acceptor Polymers. Adv. Funct. Mater. 2020, 30 (27), 2002221. DOI: 10.1002/adfm.202002221. (31) Li, Z.; Wang, Y.; Ma, G.; Liao, Y.; Gu, X.; Xia, W. Probing Conformational Properties of Conjugated Polymers in Dilute Solutions Under Variable Solvent Quality via Coarse-Grained Modeling. J. Pol. Sci 2023, Under review In press. DOI,: 10.1002/pol.20230689 Under review. Zhang, W. G.; Vargas-Lara, F.; Orski, S. V.; Beers, K. L.; Douglas, J. F. Modeling short-chain branched polyethylenes in dilute solution under variable solvent quality conditions: Basic configurational properties. Polymer 2021, 217. DOI: 10.1016/j.polymer.2021.123429. (32) Leclerc, M. Optical and electrochemical transducers based on functionalized conjugated polymers. Adv. Mater. 1999, 11 (18), 1491-+. DOI: 10.1002/(Sici)1521-4095(199912)11:18<1491::Aid-Adma1491>3.0.Co;2-O. Rughooputh, S. D. D. V.; Hotta, S.; Heeger, A. J.; Wudl, F. Chromism of soluble polythienylenes. J. Polym. Sci., Part B: Polym. Phys. 2003, 25 (5), 1071-1078. DOI: 10.1002/polb.1987.090250508. (33) McCulloch, I.; Heeney, M.; Bailey, C.; Genevicius, K.; Macdonald, I.; Shkunov, M.; Sparrowe, D.; Tierney, S.; Wagner, R.; Zhang, W.; et al. Liquid-crystalline semiconducting polymers with high charge-carrier mobility. Nat Mater 2006, 5 (4), 328-333. DOI:
- 10.1038/nmat1612.
  (34) Khasbaatar, A.; Cheng, A.; Jones, A. L.; Kwok, J. J.; Park, S. K.; Komar, J. K.; Lin, O.; Jackson, N. E.; Chen, Q.; DeLongchamp, D. M.; et al. Solution Aggregate Structures of Donor Polymers Determine the Morphology and Processing Resiliency of Non-Fullerene Organic Solar Cells. *Chem. Mater.* **2023**, *35* (7), 2713-2729. DOI: 10.1021/acs.chemmater.2c02141.
- (35) Xu, Z.; Park, K. S.; Kwok, J. J.; Lin, O.; Patel, B. B.; Kafle, P.; Davies, D. W.; Chen, Q.; Diao, Y. Not All Aggregates Are Made the Same: Distinct Structures of Solution Aggregates Drastically Modulate Assembly Pathways, Morphology, and Electronic Properties of Conjugated Polymers. *Adv Mater* **2022**, *34* (32), e2203055. DOI: 10.1002/adma.202203055.
- (36) Xue, L. J.; Yu, X. H.; Han, Y. C. Different structures and crystallinities of poly(3-hexylthiophene) films prepared from aged solutions. *Colloid Surface A* **2011**, *380* (1-3), 334-340. DOI: 10.1016/j.colsurfa.2011.03.003.
- (37) Yi, H. L.; Hua, C. C. PBTTT-C(16) sol-gel transition by hierarchical colloidal bridging. *Soft Matter* **2018**, *14* (7), 1270-1280. DOI: 10.1039/c7sm02493b.
- (38) Russo, P. S.; Streletzky, K. A.; Gorman, A.; Huberty, W.; Zhang, X. Characterization of polymers by dynamic light scattering. In *Molecular Characterization of Polymers*, Elsevier, 2021; pp 441-498. Sehgal, A.; Seery, T. A. P. Anomalous dynamic light scattering from solutions of light absorbing polymers. *Macromolecules* **1999**, *32* (23), 7807-7814. DOI: 10.1021/ma9903106.

Page 30 of 47

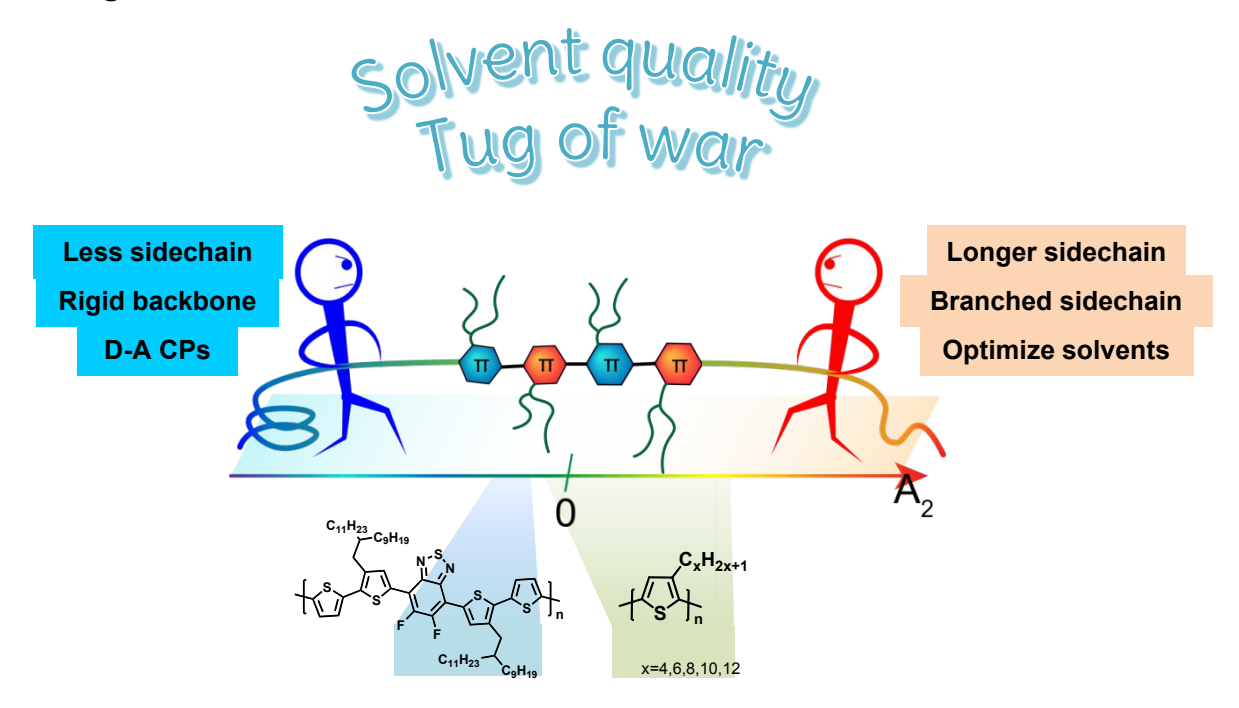
(39) Cao, Z. Q.; Ma, G. R.; Leng, M. W.; Zhang, S.; Chen, J. H.; Do, C.; Hong, K. L.; Fang, L.; Gu, X. D. Variable-Temperature Scattering and Spectroscopy Characterizations for Temperature-Dependent Solution Assembly of PffBT4T-Based Conjugated Polymers. *ACS Appl. Polym. Mater.* **2022**, *4* (5), 3023-3033. DOI: 10.1021/acsapm.1c01511. Liu, Y.; Zhao, J.; Li, Z.; Mu, C.; Ma, W.; Hu, H.; Jiang, K.; Lin, H.; Ade, H.; Yan, H. Aggregation and morphology control enables multiple cases of high-efficiency polymer solar cells. *Nat Commun* **2014**, *5*, 5293. DOI: 10.1038/ncomms6293.

Nanoscale

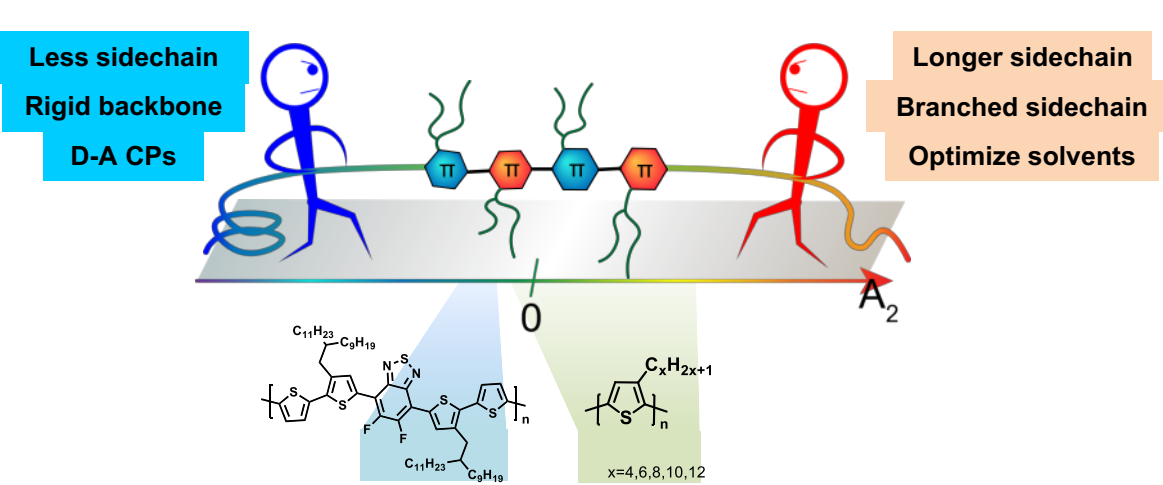
- (40) Reid, D. R.; Jackson, N. E.; Bourque, A. J.; Snyder, C. R.; Jones, R. L.; de Pablo, J. J. Aggregation and Solubility of a Model Conjugated Donor-Acceptor Polymer. *J Phys Chem Lett* **2018**, *9* (16), 4802-4807. DOI: 10.1021/acs.jpclett.8b01738.
- (41) Liao, Y. C.; Li, Z. F.; Fatima; Xia, W. J. Size-dependent structural behaviors of crumpled graphene sheets. *Carbon* **2021**, *174*, 148-157. DOI: 10.1016/j.carbon.2020.12.006. Liao, Y.; Li, Z.; Ghazanfari, S.; Fatima; Croll, A. B.; Xia, W. Understanding the Role of Self-Adhesion in Crumpling Behaviors of Sheet Macromolecules. *Langmuir* **2021**, *37* (28), 8627-8637. DOI: 10.1021/acs.langmuir.1c01545. Arkin, H.; Janke, W. Gyration tensor based analysis of the shapes of polymer chains in an attractive spherical cage. *J Chem Phys* **2013**, *138* (5), 054904. DOI: 10.1063/1.4788616 (accessed 9/22/2023).

Page 31 of 47 Nanoscale

### TOC Figure







Page 33 of 47 Nanoscale

# SI: Effect of solvent quality and sidechain architecture on the conjugated polymer chain conformation in solution

Guorong Ma<sup>1</sup>, Zhaofan Li<sup>2</sup>, Lei Fang<sup>3</sup>, Wenjie Xia<sup>2</sup>, Xiaodan Gu<sup>1\*</sup>

- 1. School of Polymer Science and Engineering, The University of Southern Mississippi, Hattiesburg, MS, 39406, USA
- 2. Department of Aerospace Engineering, Iowa State University, Ames, IA 50011, USA
- 3. Department of Chemistry, Texas A&M University, College Station, TX 77843, USA Correspondence to: Xiaodan Gu (Email: xiaodan.gu@usm.edu)

#### Table of Contents

1	EXPE	RIMENT SECTION2
	1.1	Solution preparation
	1.2	dn/dc measurement2
	1.3	HSP prediction2
	1.4	DSC measurement 2
	1	
2	SUPP	ORTING FIGURES AND TABLE
		e S1 Photo of P3ATs solutions after aging at room temperature for 2 days. The
	concer	ntration is 1.0 mg/ml
		e S2 DLS result of P3ATs at 20°C. (a, b) in THF and (c, d) in CF. The autocorrelation
		on and size distribution curve are shown in (a,c) and (b,d) respectively. The solution
		ntration is 1.0 mg/ml4
		e S3 UV-Vis absorption spectrum of all CPs in CB (a) and in Tol (b) at 20°C. The spectrum
		HT, P3OT, P3DT, and P3DDT are overlapped together4
		S1 Wavelength at maximum absorption of all solutions at 20°C4
		e S4 UV-Vis absorption spectrum of P3BT and P3HT in Tol (a, b) and CB (c, d) at various
		ratures. Solution concentration is 0.1 mg/ml
	Table	S2 Wavelength at maximum absorption of P3BT and P3HT Tol/CB solutions at various
		ratures5
		S5 UV-Vis absorption spectrum of drop cast thin films of P3BT and P3HT from Tol and
		luted solutions (0.1 mg/ml). The thin film was dried at room temperature overnight without
		al annealing6
		S4 HSP value of P3HT, PQT-12, and PBTTT-12, based on HSP prediction from HSPiP
		rre v5.4.076
		e S6 HSP value of solvent and P3HT. The arrow indicates the trend for increasing sidechain
		e. Measured HSP values of P3HT are adapted from ref <sup>1, 2</sup>
		e S7 Debye plot of P3ATs in THF (a) and CF (b)7
	Figure	e S8 DSC result of P3HT, PQT-12 and PBTTT-12. Curves are from the second heating scan
		heating rate of 10K/min
		e S9 DLS evolution of P3HT solution 1.0 mg/ml after aging at r.t. for 10 days under dark
		ions. Autocorrelation curve of P3HT in CB (a) and Tol (b), and particle size distribution in
		and Tol (d) by NNLS fitting8
		e S10 Sideview of an incidence laser beam (left) passing through a toluene solvent (a) and
		ng/ml PffBT4T-C9C13 chlorobenzene solutions (b). (c) Photos of transmission laser
		ted on an A4 paper 1.5m away after passing through solution described in (b)
		e S11 (a) Polymer architectures of type V and VI. (b-c) Reduced $R_g$ of polymer chain as a
	function	on of solvent quality for type V to VI, respectively9
	Figure	S12 Normalized squared radius of gyration $R_g^2/(N-1)$ as a function of solvent quality $\lambda$
		lymer models I to VI, respectively, at higher temperatures. The location of the $\theta$ point is
		ted by the black dashed line
		$\sim$ S13 The persistence length $L_{\rm p}$ as a function of varying solvent quality $\lambda$ for polymer
		s type I to VI, respectively11
		e S14 Normalized squared end-to-end distance $R_{ee}^2/(N-1)$ as a function of solvent quality
	λ for p	polymer models type I to VI, respectively
	Figure	S15 The shape descriptor $\underline{\kappa 2}$ as a function of varying solvent quality $\lambda$ for polymer
	model	s type I to VI, respectively

Page 35 of 47 Nanoscale

Figu	e S16 Molecular mass dependence of radius of gyration $R_{ m g}$ for solvent qualities ran	ging
fron	an ideal good solvent, $\theta$ solvent, to a poor solvent for seven types of polymer architecture.	tectures.
••••		14
REFERE	CE	14

#### 1 Experiment section

#### 1.1 Solution preparation

Polymers were dissolved in filtered solvents and heated up to 80°C overnight to ensure fully dissolved.

#### 1.2 dn/dc measurement

20 mg CPs were dissolved in 1.0 ml solvents to obtain 20 mg/ml concentrated solution. Solution refractive index was measured by Abbe refractometry (Mettler Toledo Easy R40) at 20±0.1°C and the differential refractive index was determined by the following equation.

$$\frac{dn}{dc} = \frac{n_{solution} - n_{solvent}}{c}$$
 Eq.1

#### 1.3 HSP prediction

HSP values for CPs and solvents are obtained from prediction in HSPiP software v5.4.07 shown in **Figure S6** and **Table S4**. Note that the predicted HSP value of P3HT does not match with the experimental value<sup>1</sup>. And no other P3ATs' HSP value has been measured and reported to the best of our knowledge.

#### 1.4 DSC measurement

Differential scanning calorimetry (DSC) was performed in the Mettler Toledo 3+ DSC instrument. About 3 mg samples were sealed into an aluminum pan and the heating and cooling rate was 10 °C/min under  $N_2$  flow.

#### 2 Supporting figures and table

Nanoscale Page 36 of 47

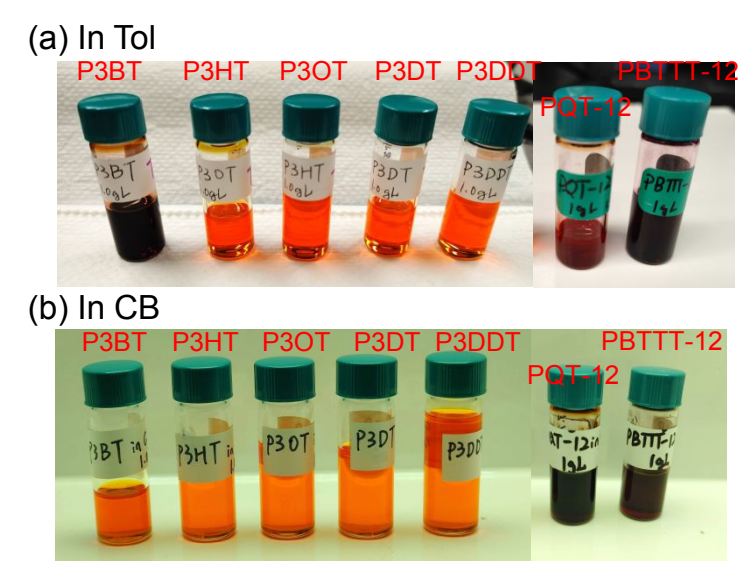


**Figure S1** Photo of P3ATs solutions after aging at room temperature for 2 days. The concentration is 1.0 mg/ml.

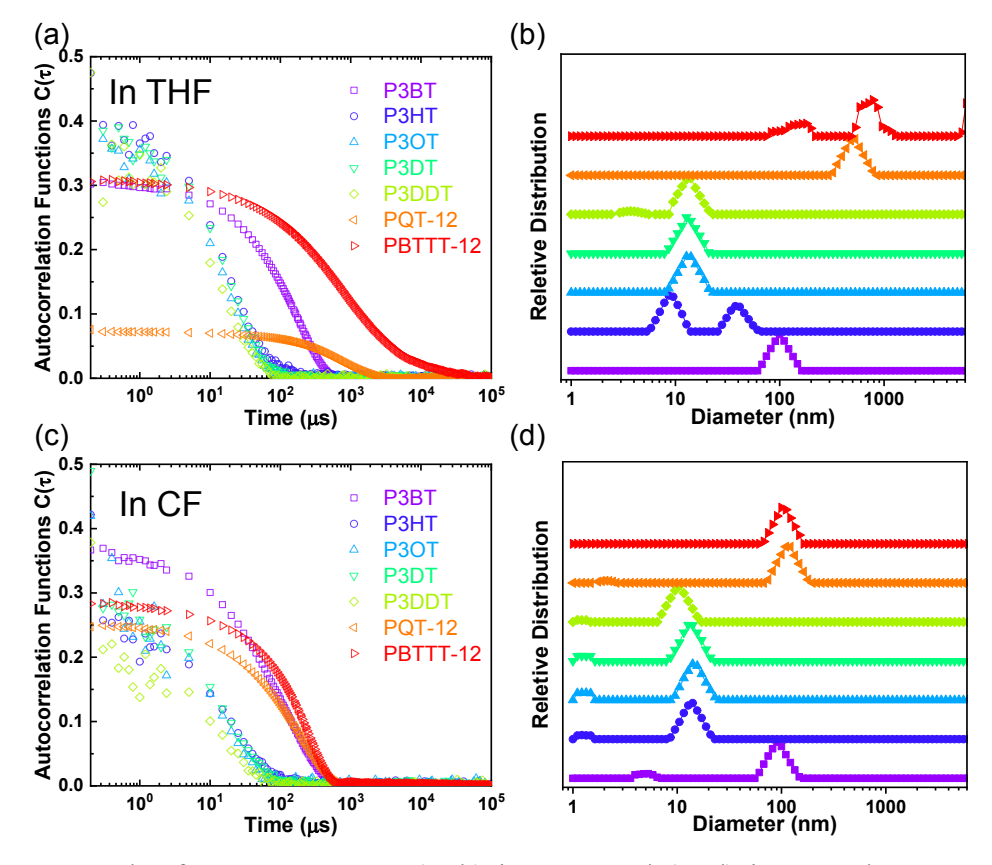


**Figure S2** DLS result of P3ATs at 20°C. (a, b) in THF and (c, d) in CF. The autocorrelation function and size distribution curve are shown in (a,c) and (b,d) respectively. The solution concentration is 1.0 mg/ml.

Page 37 of 47 Nanoscale

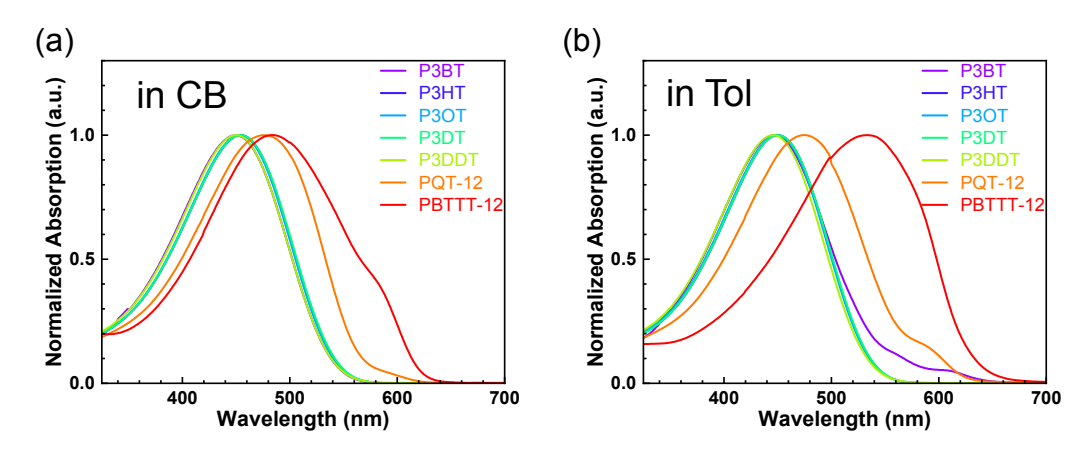


**Figure S3** UV-Vis absorption spectrum of all CPs in CB (a) and in Tol (b) at 20°C. The spectrum of P3HT, P3OT, P3DT, and P3DDT are overlapped together.

**Table S1** Wavelength at maximum absorption of all solutions at 20°C.

Name	λ <sub>max abs, CB</sub> /nm	λ <sub>max abs, Tol</sub> /nm
P3BT	449	446
P3HT	454	450
P3OT	453	449
P3DT	454	450
P3DDT	450	446
PQT-12	476	474
PBTTT-12	483	533

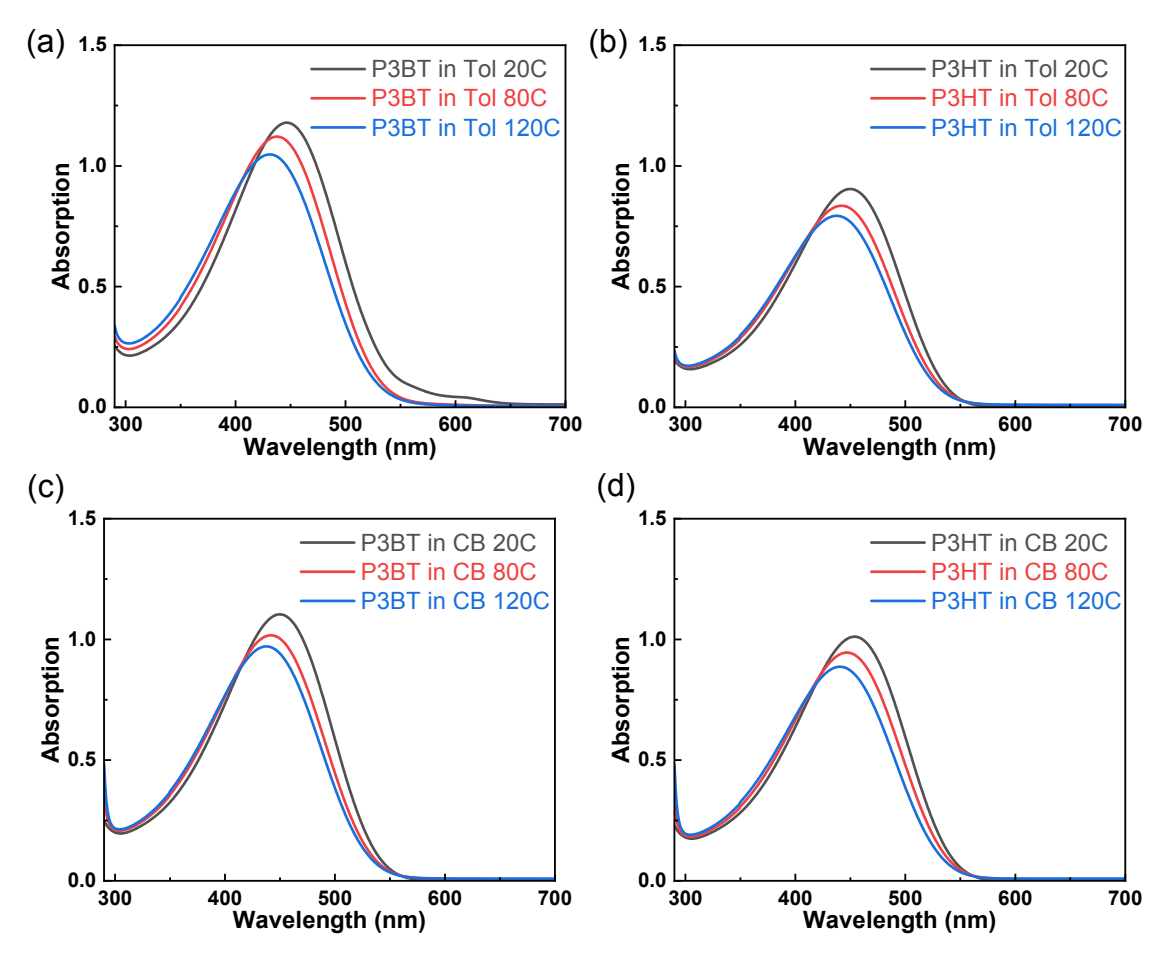


**Figure S4** UV-Vis absorption spectrum of P3BT and P3HT in Tol (a, b) and CB (c, d) at various temperatures. Solution concentration is 0.1 mg/ml.

**Table S2** Wavelength at maximum absorption of P3BT and P3HT Tol/CB solutions at various temperatures.

Polymer	Temperature/°C	λ <sub>max abs, Tol</sub> /nm	λ <sub>max abs, CB</sub> /nm
	20	447	450
P3BT	80	438	442
	120	431	438
	20	450	454
P3HT	80	442	447
	120	437	441

Page 39 of 47 Nanoscale

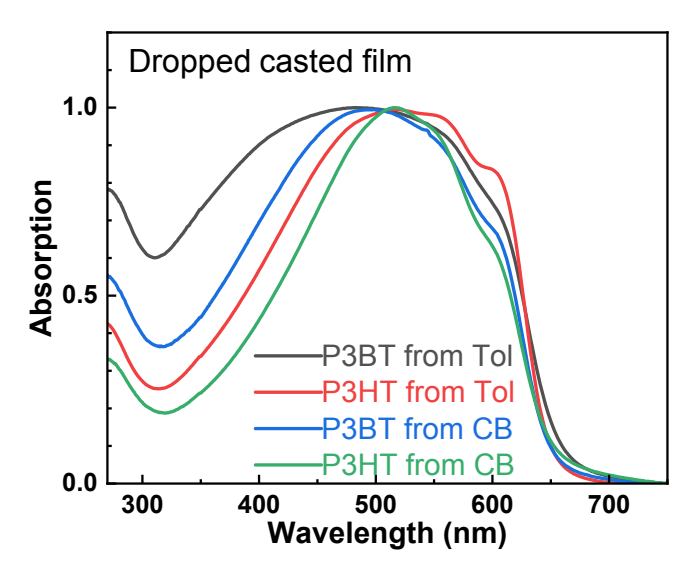


**Figure S5** UV-Vis absorption spectrum of drop cast thin films of P3BT and P3HT from Tol and CB diluted solutions (0.1 mg/ml). The thin film was dried at room temperature overnight without thermal annealing.

**Table S3** dn/dc value (at Na D line) and absorption coefficient (at 633nm) value of P3ATs in various solvents. \*PQT-12 and PBTTT-12 are assumed to be the same as P3HT due to the difficulties of their measurement.

Polymer/	dn/dc (ml/g)			
Solvent	СВ	Toluene	THF	Chloroform
P3BT	0.280	0.225	0.465	0.365
P3HT	0.225	0.195	0.320	0.305
P3OT	0.175	0.200	0.420	0.295
P3DT	0.150	0.180	0.315	0.235
P3DDT	0.125	0.155	0.335	0.210
PQT-12*	0.225	0.195	0.320	0.305
PBTTT-12*	0.225	0.195	0.320	0.305

**Table S4** HSP value of P3HT, PQT-12, and PBTTT-12, based on HSP prediction from HSPiP software v5.4.07.

Polymer Name		Р3НТ	PQT-C12	PBTTT-C12
Formula		$(C_{40}H_{56}S_4)n$	$(C_{40}H_{56}S_4)n$	$(C_{38}H_{56}S_4)n$
	δD	15.9	16.8	15.9
Prediction by HSPiP	δP	1.2	1.2	1.5
	δН	2.1	2.1	1.8

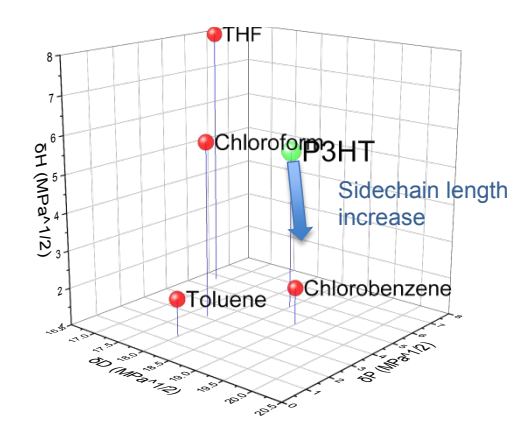


**Figure S6** HSP value of solvent and P3HT. The arrow indicates the trend for increasing sidechain volume. Measured HSP values of P3HT are adapted from ref<sup>1, 2</sup>.

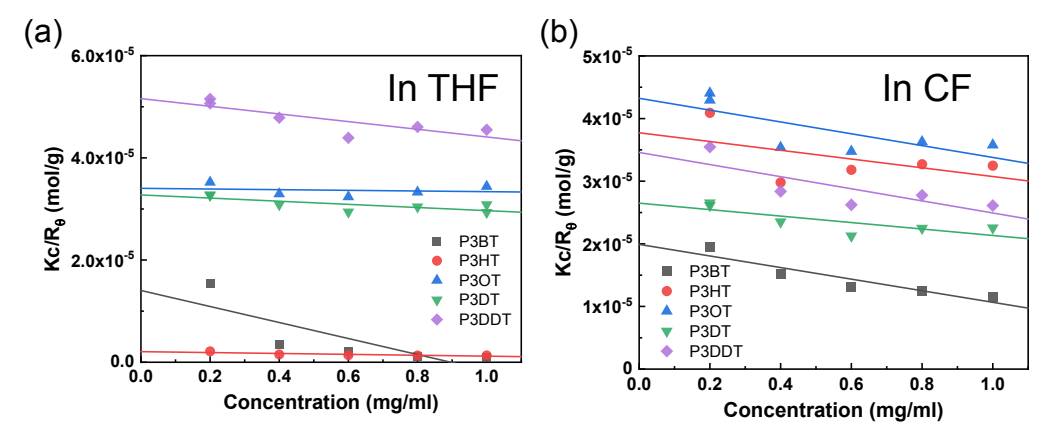
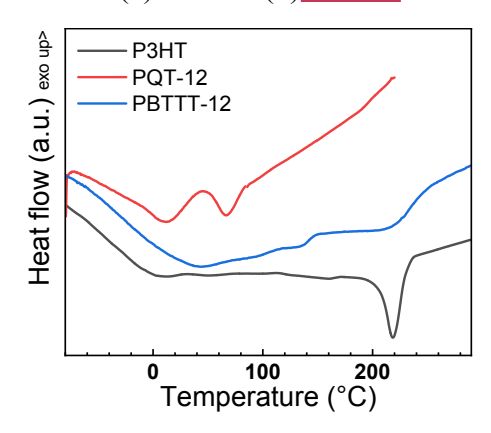
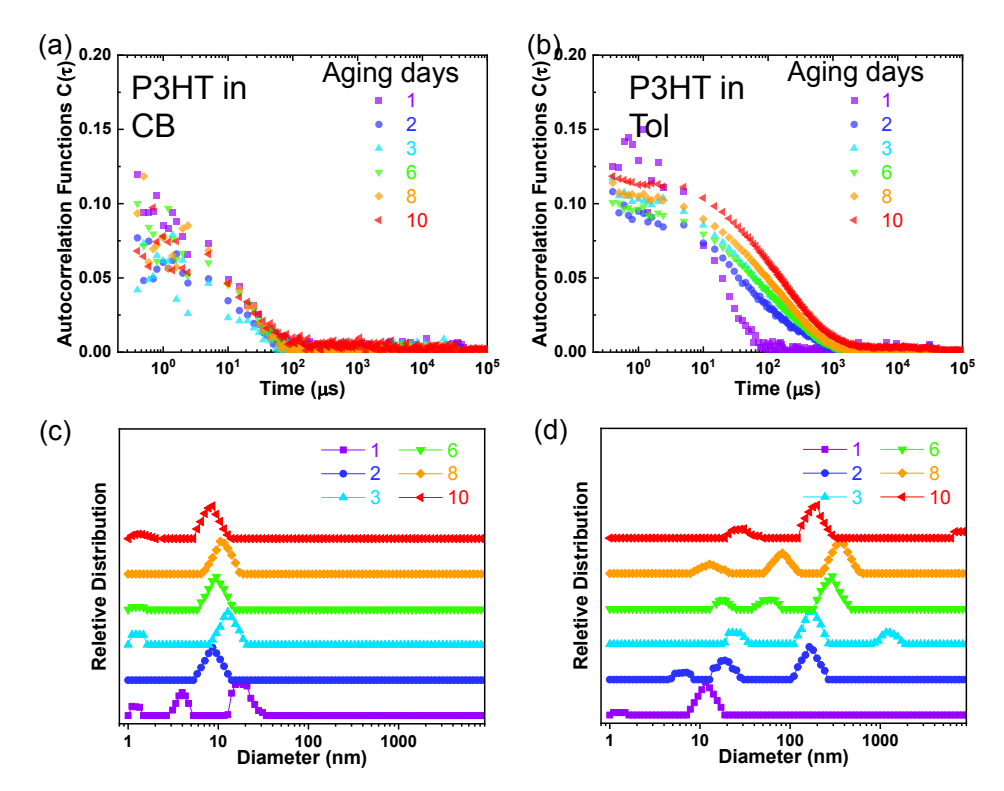


Figure S7 Debye plot of P3ATs in THF (a) and CF (b) at 20°C.



**Figure S8** DSC result of P3HT, PQT-12 and PBTTT-12. Curves are from the second heating scan with a heating rate of 10K/min.

Page 41 of 47 Nanoscale



**Figure S9** DLS evolution of P3HT solution 1.0 mg/ml after aging at r.t. for 10 days under dark conditions. Autocorrelation curve of P3HT in CB (a) and Tol (b), and particle size distribution in CB (c) and Tol (d) by NNLS fitting.

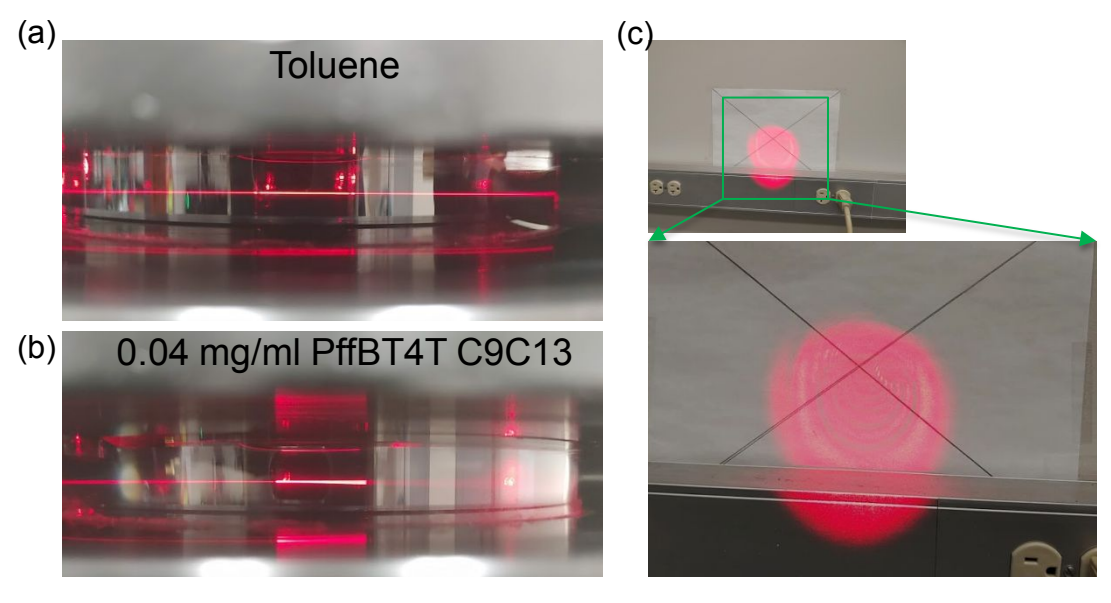


**Figure S10** Sideview of an incidence laser beam (left) passing through a toluene solvent (a) and 0.04 mg/ml PffBT4T-C9C13 chlorobenzene solutions (b). (c) Photos of transmission laser projected on an A4 paper 1.5m away after passing through solution described in (b).

Nanoscale Page 42 of 47

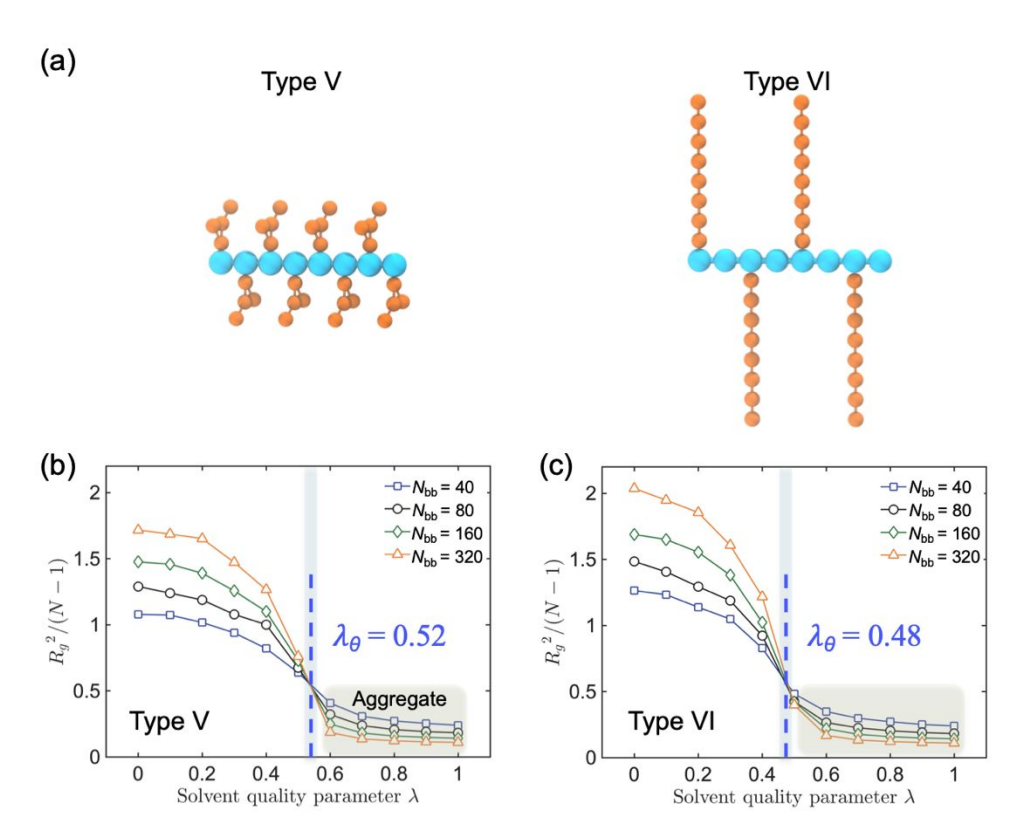


**Figure S11** (a) Polymer architectures of type V and VI. (b-c) Reduced  $R_g$  of polymer chain as a function of solvent quality for type V to VI, respectively.

Page 43 of 47 Nanoscale

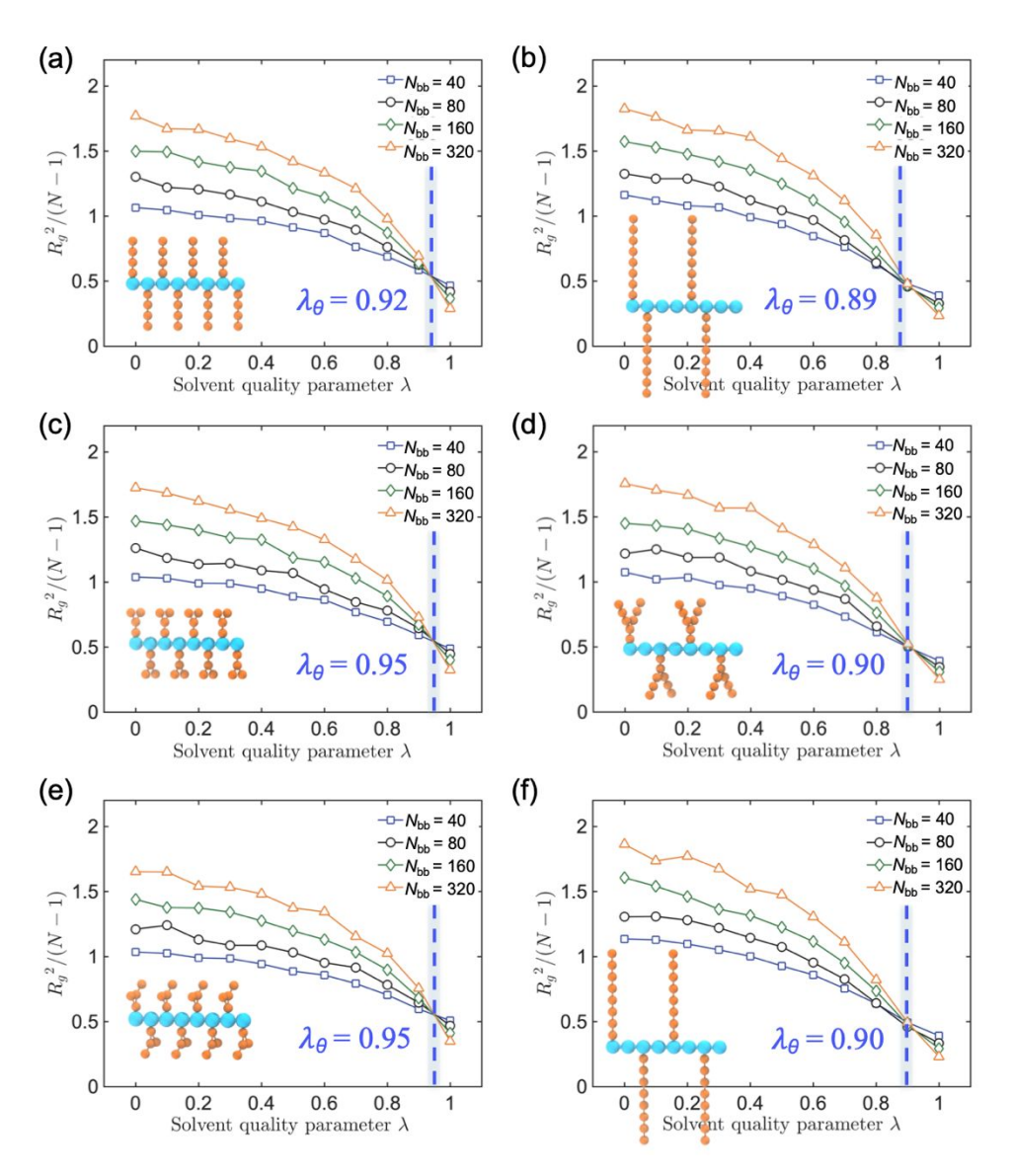


**Figure S12** Normalized squared radius of gyration  $R_g^2/(N-1)$  as a function of solvent quality  $\lambda$  for polymer models I to VI, respectively, at higher temperatures. The location of the  $\theta$  point is indicated by the black dashed line.

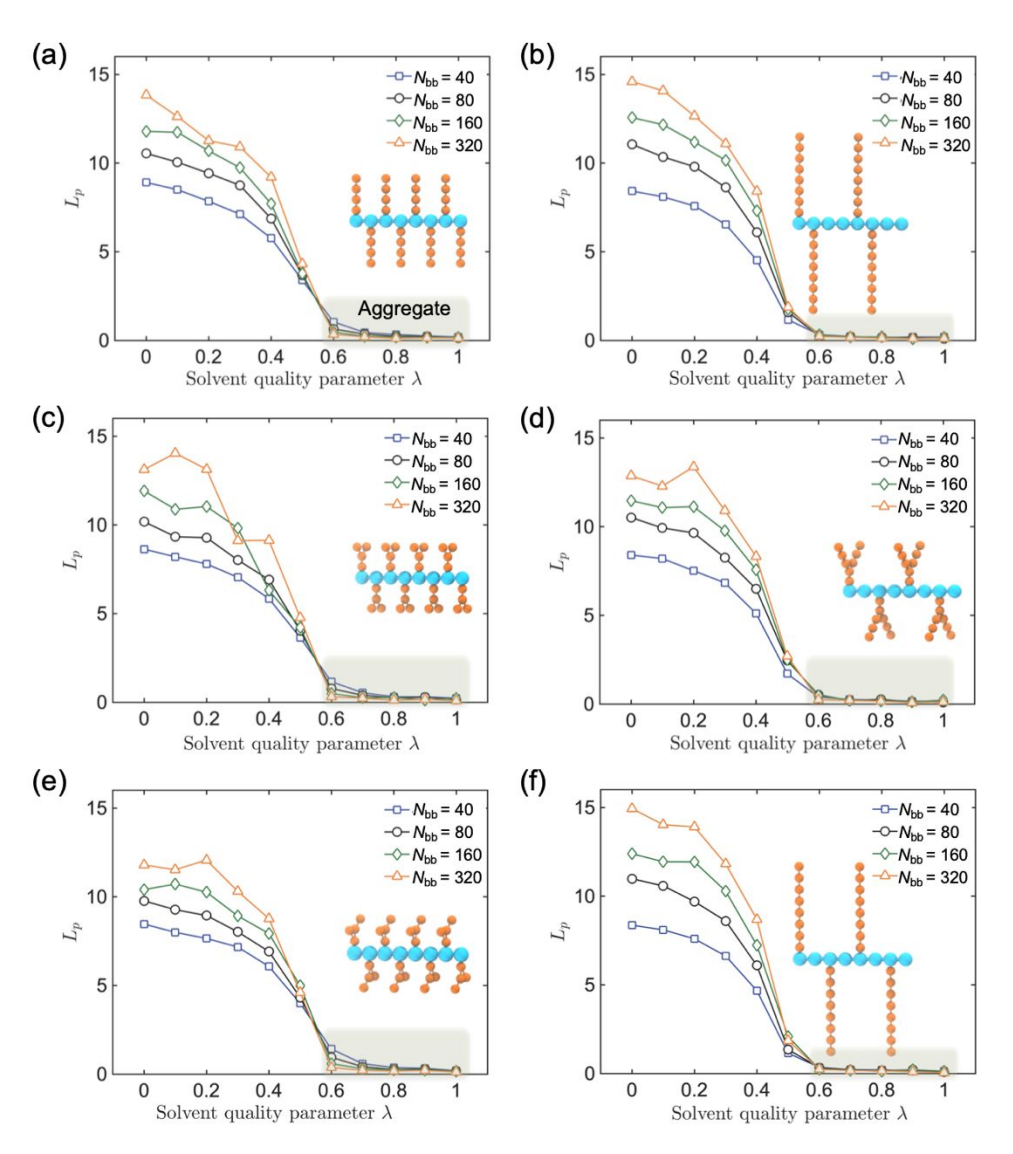


**Figure S13** The persistence length  $L_p$  as a function of varying solvent quality  $\lambda$  for polymer models type I to VI, respectively.

Page 45 of 47 Nanoscale

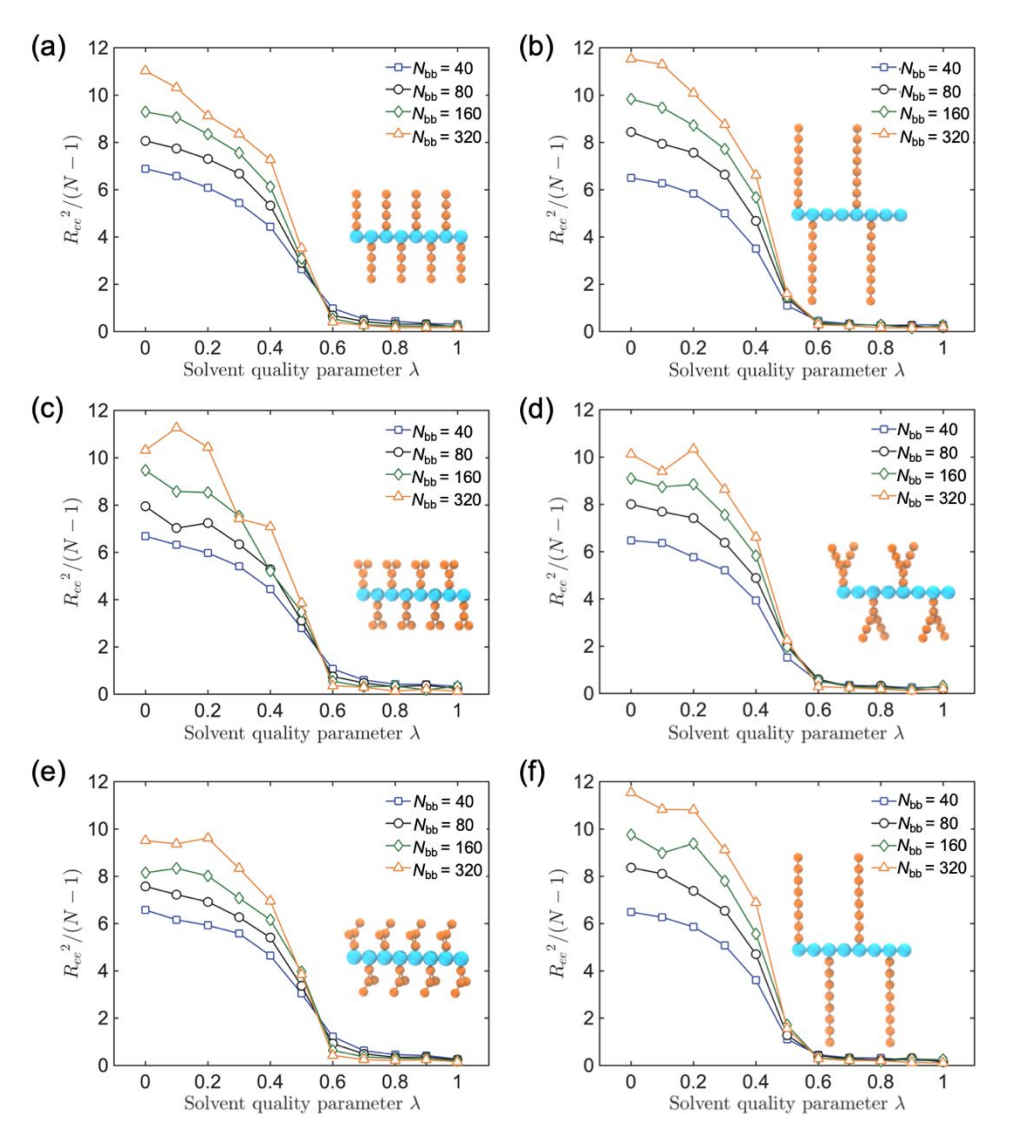


**Figure S14** Normalized squared end-to-end distance  $R_{ee}^2$  / (N - 1) as a function of solvent quality  $\lambda$  for polymer models type I to VI, respectively.

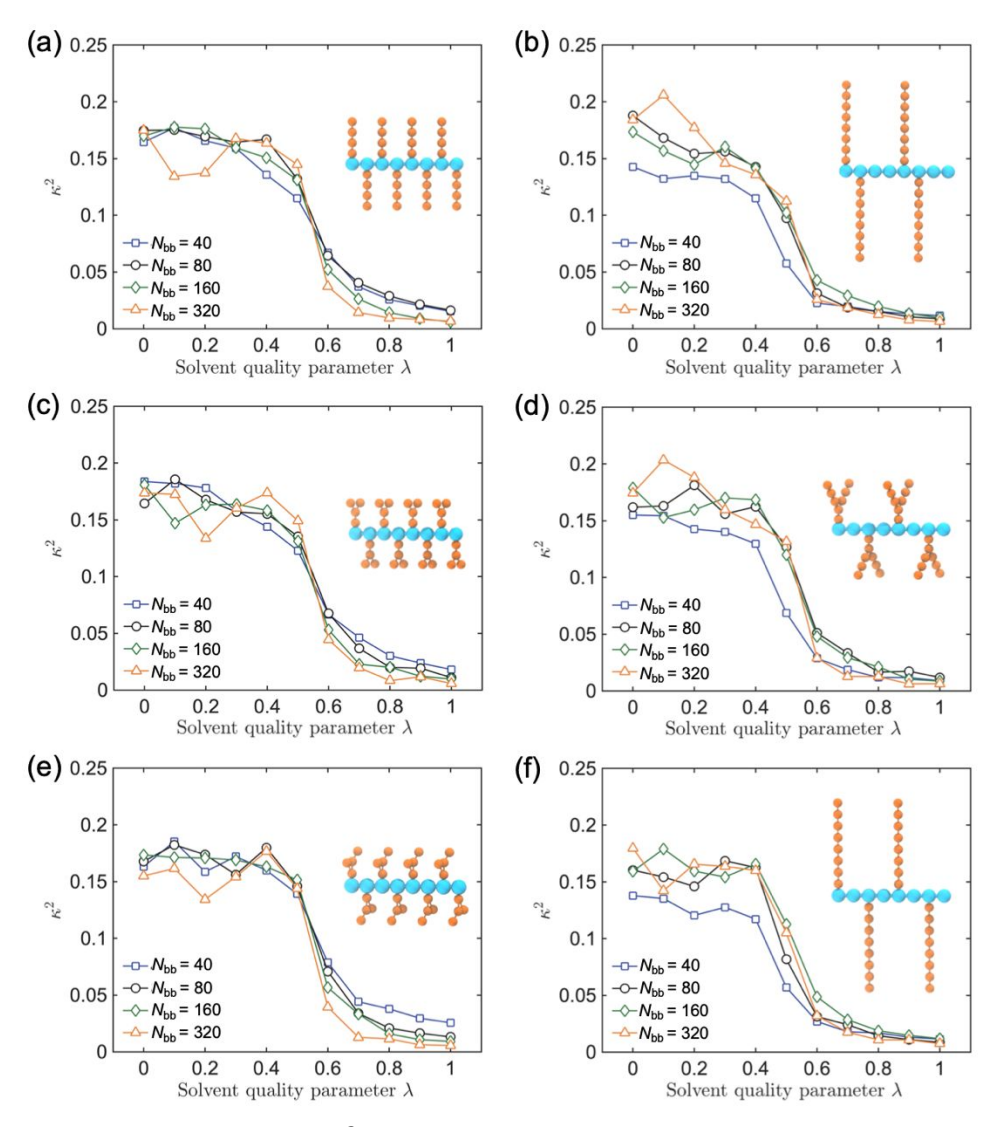


**Figure S15** The shape descriptor  $\kappa^2$  as a function of varying solvent quality  $\lambda$  for polymer models type I to VI, respectively.

Page 47 of 47 Nanoscale

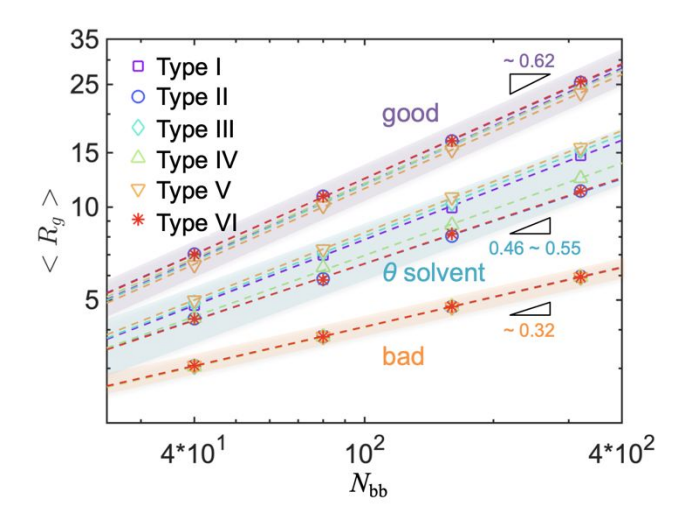


Figure S16 Molecular mass dependence of radius of gyration  $R_g$  for solvent qualities ranging from an ideal good solvent,  $\theta$  solvent, to a poor solvent for seven types of polymer architectures. Reference

- 1. Machui, F.; Langner, S.; Zhu, X. D.; Abbott, S.; Brabec, C. J. Determination of the P3HT:PCBM solubility parameters via a binary solvent gradient method: Impact of solubility on the photovoltaic performance. *Sol. Energy Mater. Sol. Cells* **2012**, 100, 138-146 DOI: 10.1016/j.solmat.2012.01.005.
- 2. Machui, F.; Abbott, S.; Waller, D.; Koppe, M.; Brabec, C. J. Determination of Solubility Parameters for Organic Semiconductor Formulations. *Macromol. Chem. Phys.* **2011**, 212 (19), 2159-2165 DOI: 10.1002/macp.201100284.